Available online at www.sciencedirect.com
ScienceDirect
Geochimica et Cosmochimica Acta 73 (2009) 183–196
Geochimica et Cosmochimica Acta
www.elsevier.com/locate/gca

The influence of artificial radiation damage and thermal annealing on helium diffusion kinetics in apatite

David L. Shuster [a,*], Kenneth A. Farley [b]

[a] Berkeley Geochronology Center, 2455 Ridge Road, Berkeley, CA 94709, USA
[b] Department of Geological and Planetary Sciences, MS 170-25, Caltech, Pasadena, CA 91125, USA

Received 15 July 2008; accepted in revised form 10 October 2008; available online 21 October 2008

Abstract

Recent work [Shuster D. L., Flowers R. M. and Farley K. A. (2006) The influence of natural radiation damage on helium diffusion kinetics in apatite. *Earth Planet. Sci. Lett.* **249**(3–4), 148–161] revealing a correlation between radiogenic ^{4}He concentration and He diffusivity in natural apatites suggests that helium migration is retarded by radiation-induced damage to the crystal structure. If so, the He diffusion kinetics of an apatite is an evolving function of time and the effective uranium concentration in a cooling sample, a fact which must be considered when interpreting apatite (U–Th)/He ages. Here we report the results of experiments designed to investigate and quantify this phenomenon by determining He diffusivities in apatites after systematically adding or removing radiation damage.

Radiation damage was added to a suite of synthetic and natural apatites by exposure to between 1 and 100 h of neutron irradiation in a nuclear reactor. The samples were then irradiated with a 220 MeV proton beam and the resulting spallogenic ^{3}He used as a diffusant in step-heating diffusion experiments. In every sample, irradiation increased the activation energy (E_a) and the frequency factor (D_o/a^2) of diffusion and yielded a higher He closure temperature (T_c) than the starting material. For example, 100 h in the reactor caused the He closure temperature to increase by as much as 36 °C. For a given neutron fluence the magnitude of increase in closure temperature scales negatively with the initial closure temperature. This is consistent with a logarithmic response in which the neutron damage is additive to the initial damage present. In detail, the irradiations introduce correlated increases in E_a and $\ln(D_o/a^2)$ that lie on the same array as found in natural apatites. This strongly suggests that neutron-induced damage mimics the damage produced by U and Th decay in natural apatites.

To investigate the potential consequences of annealing of radiation damage, samples of Durango apatite were heated in vacuum to temperatures up to 550 °C for between 1 and 350 h. After this treatment the samples were step-heated using the remaining natural ^{4}He as the diffusant. At temperatures above 290 °C a systematic change in T_c was observed, with values becoming lower with increasing temperature and time. For example, reduction of T_c from the starting value of 71 to ~52 °C occurred in 1 h at 375 °C or 10 h at 330 °C. The observed variations in T_c are strongly correlated with the fission track length reduction predicted from the initial holding time and temperature. Furthermore, like the neutron irradiated apatites, these samples plot on the same $E_a - \ln(D_o/a^2)$ array as natural samples, suggesting that damage annealing is simply undoing the consequences of damage accumulation in terms of He diffusivity.

Taken together these data provide unequivocal evidence that at these levels, radiation damage acts to retard He diffusion in apatite, and that thermal annealing reverses the process. The data provide support for the previously described radiation damage trapping kinetic model of Shuster et al. (2006) and can be used to define a model which fully accommodates damage production and annealing.

* Corresponding author.
E-mail address: dshuster@bgc.org (D.L. Shuster).

0016-7037/$ - see front matter © 2008 Elsevier Ltd. All rights reserved.
doi:10.1016/j.gca.2008.10.013

1. INTRODUCTION

Application of (U–Th)/He cooling ages to the solution of geologic problems requires that helium diffusion kinetics quantified in the laboratory be accurately extrapolated to conditions of interest in nature, specifically to lower temperatures and over geologic timescales. The recent suggestions that naturally occurring radiation damage modifies He diffusion in apatite (Farley, 2000; Crowley et al., 2002; Green et al., 2006; Green and Duddy, 2006; Shuster et al., 2006) underscore the challenge of this extrapolation: helium diffusivity is an evolving function of time governed by both temperature and effective uranium concentration (*eU*) (Shuster et al., 2006; Flowers et al., 2007). In this study we present results of controlled experiments in which we explore the response of He diffusion in apatite to increases in crystal damage caused by artificial irradiation, and to annealing of damage at elevated temperatures. In a subsequent publication, we will investigate the implications of these observations for apatite He thermochronometry.

The interactions between radiation and crystalline matter involve ionizations, nuclear transmutations and direct scattering displacements of constituent atoms (Ewing et al., 1995; Weber et al., 1998). Based on the total *number* of atomic displacements per unit time, the most important of these interactions for He diffusion in minerals is likely from alpha recoil of heavy nuclei in the ^{238}U, ^{235}U, and ^{232}Th decay chains (Weber et al., 1997; Trachenko et al., 2002), but may also include the effects of the alpha particles themselves and spontaneous U fission. Regardless of source, the resulting displacements (Ewing et al., 1995) can modify the energetic environment along diffusion pathways and may either impede or promote diffusion. In a suite of natural apatites, He diffusivities below ~200 °C decrease with increasing radiation damage (Shuster et al., 2006). This leads to the idea of a radiation damage "trap", a local damaged region of the lattice in which He is preferentially sited. Diffusion through a radiation-damaged crystal involves two energetic terms: one to escape the damaged site, and another to migrate through the undamaged lattice. This model predicts a log-linear relationship between the volume fraction of radiation damage in an apatite and the helium closure temperature; (Shuster et al., 2006) documented such a correlation in a suite of natural apatites using ^{4}He as a proxy for radiation damage (Fig. 1). These data provided the calibration for a kinetic model for He diffusion that includes both temperature and radiation damage as independent variables (black curve in Fig. 1).

At high enough radiation doses many solids approach an aperiodic or glasslike state. Previous work shows that zircons and titanites that reach such a state diffuse He very rapidly (Hurley, 1952, 1954; Nasdala et al., 2004). The fact that apatite tends to have lower concentrations of U and Th and has a greater propensity to anneal radiation damage may prevent it from reaching this condition, although at present there are insufficient data to know.

Annealing or reversion of damaged sites back to a crystalline state occurs in many solids. The rate of this process depends on many variables including temperature, the volume fraction of damaged sites, and chemical and mineralogical composition. Limited work on apatite (Farley, 2000) suggests that annealing enhances He diffusion, as would be expected if the radiation damage traps are eliminated by this process. At present we have insufficient data to quantify how annealing influences He diffusion in apatite or any other mineral. The radiation damage trapping model of Shuster et al. (2006) included this effect only in an indirect manner.

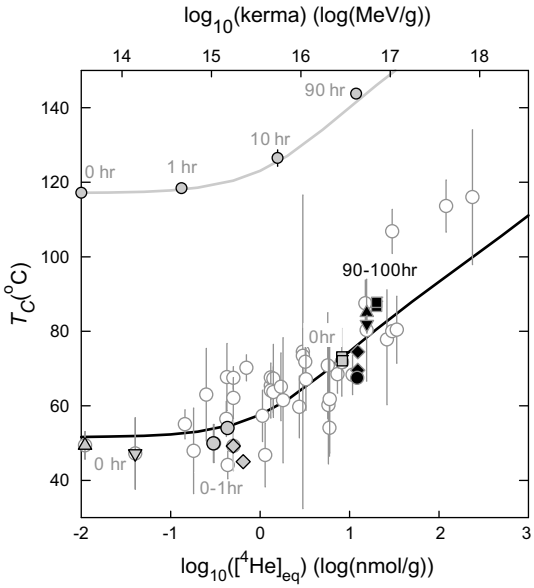

Fig. 1. Neutron irradiation experiments: Helium closure temperature (T_c) versus the log of the concentration of equivalent ^{4}He ($\log_{10}([^{4}He]_{eq})$ and the total kinetic energy released into matter ($\log_{10}$(kerma)), as described in the text. Values of T_c were calculated for a cooling rate of 10 °C/Ma using the formulation of Fechtig and Kalbitzer (1966) for diffusion kinetics determined from stepwise release fractions of proton-induced ^{3}He or natural radiogenic ^{4}He. We estimated uncertainty in T_c (1σ; shown as vertical lines) solely from the linear regression statistics from the Arrhenius plots. The open, light-gray circles correspond to natural apatites and the solid black curve is the "trapping model" from Shuster et al. (2006). The gray circles plotting between $T_c \sim 120$ and 140 °C are the results of neutron irradiation experiments on a synthetic fluorapatite sample shown in Fig. 2a. The dark gray points (0 and 1 h irradiations) and black points (90 and 100 h irradiations) correspond to the five neutron irradiation experiments conducted on a suite of natural apatites summarized in Table 1 and shown in Fig. 2b and c and Fig. EA1. Up triangles = CJ50, down triangles = 00mr18, circles = DYJS5, diamonds = 01mr59, squares = Durango. Times correspond to number of hours in the CLICIT facility within the nuclear reactor (see text).

For thermochronometry, we are most interested in the extensive properties of the damaged material, i.e., the effective bulk diffusivity of the material at a given point in time. Our goal in this work is to confirm and quantify the effects of damage accumulation and annealing on the kinetics of helium diffusion, rather than illuminate details at the atomic scale. Our approach is twofold. First, to simulate the effects of natural radiation damage we subjected apatites to neutron irradiation, a technique by which to induce variable and controlled amounts of lattice damage comparable

to that produced by alpha recoil. Second, we subjected a natural apatite to a suite of experimental conditions at which lattice annealing is known to occur to varying extents. After these treatments we made routine stepped-heating measurements on the samples to quantify the resulting changes in He diffusion kinetics. Throughout this paper, we focus on the closure temperature (T_c) as a parameter which encapsulates the combined effects of modifying both E_a and D_o/a^2 in our experiments. However, ultimately it is these two fundamental parameters of diffusion (rather than T_c) that are both directly observable in an Arrhenius plot *and* most relevant for quantifying He diffusivity on laboratory and geologic time scales.

2. SAMPLES AND METHODS

2.1. Samples

The well-studied helium diffusivity (Zeitler et al., 1987; Wolf et al., 1996; Farley, 2000) and annealing behavior (Green, 1988; Carlson et al., 1999; Ravenhurst et al., 2003) of the fluorapatite from Cerro de Mercado, Durango, Mexico (Young et al., 1969) make it a logical choice to investigate here. Our specimen of Durango consists of fragments produced by crushing a slab cut from the interior of a large, gem-quality megacryst. Two different grain sizes of Durango were analyzed. Most experiments were done on shards of a standard we call CIT Dur-B, sieved to a mean cross section of ~170 μm. This fraction is from the same megacryst and is similar in size to the CIT Dur-A material studied previously at Caltech and currently used as an age standard (Farley, 2000). Dur-A shards have a helium closure temperature, $T_c = 71.7 \pm 1.9$ °C (here and below assuming $dT/dt = 10$ °C/Myr). For a few experiments we analyzed aliquots that consisted of a single large (few mm) chip from the same Durango megacryst.

Only Durango was investigated in the annealing experiments, but the irradiation experiments were performed on Dur-B as well as four natural apatites from granitoid rocks and a synthetic fluorapatite. The synthetic fluorapatite (WSAp) was synthesized in a flux of CaF_2 (Prener, 1967; Cherniak, 2005). The analyzed crystals had a mean cross section of ~300 μm, and we assume that this material initially contains no radiation damage. Helium diffusion kinetics and compositional data for the four granitoid apatites were reported earlier (Shuster et al., 2005, 2006). They were selected for neutron irradiation experiments because they have significantly lower helium retentivity than Durango apatite (T_c for 01mr59 = 49.2 ± 6.6 °C, DYJS5 = 49.9 ± 5.1 °C, CJ50 = 49.4 ± 3.7 °C (CJ50), and 00mr18 = 47.2 ± 9.6 °C). The lower He retentivity in these samples is consistent with a relatively low volume fraction of radiation damage and suggests these samples will be readily affected by the addition of damage from neutron irradiation. Mean cross sections of the analyzed grains range from ~95 to 120 μm.

2.2. Initial treatment: neutron irradiation–proton irradiation

To induce radiation damage the six samples were loaded into an Al disk (routinely used for $^{40}Ar/^{39}Ar$ dating), and held within the cadmium lined in-core irradiation tube (CLICIT) facility of the Oregon State University TRIGA nuclear reactor for 1, 10, 90, or 100 h. The samples were subjected to a 1 MeV equivalent neutron fluence ($\Phi_{eq,\ 1MeV,\ Si}$) equal to $\sim 2.3 \times 10^{16}$, $\sim 2.7 \times 10^{17}$, $\sim 2.0 \times 10^{18}$, and $\sim 2.7 \times 10^{18}$ n/cm^2, respectively. We calculated these values of $\Phi_{eq,\ 1MeV,\ Si}$ from an external calibration of the CLICIT facility (referenced to silicon) using conventional techniques (ASTM, 1994). The energy spectrum within the CLICIT is dominated by moderate energies; roughly 50% of the incident neutrons have energy between 1 and 4 MeV (Figs. EA3 and EA4). We expect the higher energy neutrons to induce a greater proportion of damage than those at lower energies. For the 90 and 100 h irradiations, the samples were not continuously exposed to the neutron flux. The 90 h irradiation was conducted in ~33 consecutive steps between January 23 and February 23, 2006, and the 100 h irradiation was conducted in 21 consecutive steps between November 29 and January 3, 2007.

Following the neutron irradiations, these samples were subjected to proton irradiation at *The Francis H. Burr Proton Therapy Center* at Massachusetts General Hospital to produce a uniform spatial distribution of ^{3}He using previously published procedures (Shuster et al., 2004). For these experiments we used a 220 MeV proton beam and a fluence of $\sim 5 \times 10^{16}$ p/cm^2. The irradiations took place over a continuous ~8 h period on either April 30, 2006 or October 21, 2007.

Note that the Durango aliquots used in the annealing experiments (see below) were neither neutron irradiated nor proton irradiated.

2.3. Initial treatment: thermal annealing

A suite of experiments was undertaken to assess whether ^{4}He diffusion is modified when apatite is heated to temperatures at which radiation damage annealing is expected based on fission track annealing kinetics (e.g., Green, 1988). For these experiments ~5–30 mg aliquots of Dur-B or Durango chips were loaded in copper foil pouches and heated in vacuum using a projector lamp apparatus (Farley et al., 1999). This device is capable of rapid temperature cycling and has an estimated temperature uncertainty of less than 2 °C.

Annealing durations were between 1 and 350 h at temperatures ranging from 20 to 500 °C. During the annealing step the evolved He was accumulated, then analyzed using isotope dilution quadrupole mass spectrometry as described elsewhere (Farley, 2000). Following the annealing step the sample was subjected to a routine diffusion coefficient step-heat experiment without breaking vacuum (see Section 2.4).

2.4. Diffusion experiments

For the neutron irradiation experiments, we quantified helium diffusion kinetics using stepped-release of proton-induced ^{3}He (Shuster et al., 2004), while for the annealing experiments we used the residual natural ^{4}He as the diffusant (Wolf et al., 1996; Farley et al., 1999; Shuster et al.,

2004). Aliquots ranging in size from a single crystal to many mg were held at a controlled temperature for a known time in a chamber under static vacuum (Farley et al., 1999). After heating, evolved helium was purified and cryogenically separated from other noble gases using activated charcoal held at 32 K and analyzed using either a sector-field mass spectrometer at BGC (^{3}He) or a quadrupole mass spectrometer at Caltech (^{4}He). Using the fraction of ^{3}He or ^{4}He released and the duration of each step, we calculated the diffusion coefficient (D) normalized to the characteristic diffusive length scale a, (i.e., D/a^2) using published equations and the assumptions therein (Fechtig and Kalbitzer, 1966).

We report D/a^2 values (rather than D values) for all of our samples. The only exception is for the Durango large chip experiments in which we scaled from the D/a^2 values actually measured to $a = 85$ μm (equivalent to Dur-B) using the measured grain dimensions and an equivalent sphere model (Meesters and Dunai, 2002). Given the complicated geometry of the analyzed chips this computation is fairly uncertain, so these data, especially the D/a^2 and closure temperature values, are deemed less reliable than those obtained on Dur-B.

We quantified the temperature dependence of the diffusion coefficient from a series of steps on each sample. Such data permit linear regression of $\ln(D/a^2)$ against $1/T$ assuming the Arrhenius relationship $D(T)/a^2 = D_o/a^2 \exp(-E_a/RT)$, where E_a is the activation energy, D_o is the diffusivity at infinite temperature, and R is the gas constant. The heating schedule and data selection criteria used in the regressions are described in the next section.

In calculating and interpreting our data we are explicitly assuming that ^{3}He and ^{4}He diffusion kinetics are interchangeable despite a substantial mass difference. Previous works suggests this conclusion is valid for apatite (Shuster et al., 2004). Similarly, other than for the coarse Durango chips for which we are certain we can (and must) scale diffusivity from one grain size to another (Farley, 2000), we are making no adjustments for the small grain size differences among our samples. This follows the approach of our previous work in which the small range of grain sizes routinely analyzed for He dating yields variations in diffusivity far smaller than variations caused by the factors of interest in the present study (Shuster et al., 2006). The issue of grain size will be considered further in a subsequent publication.

2.4.1. Heating schedule and regression criteria for neutron irradiated samples

The heating schedule for the synthetic apatites began with a set of isothermal steps at either 150 or 250 °C continuing with sets of isothermal steps up to 600 °C. All of the natural samples were analyzed using a heating schedule starting with at least 3 isothermal extractions at 200 °C, followed by a series of decreasing temperature (retrograde) steps, followed by increasing temperature (prograde) steps up to 600 °C. Beginning our experiments at moderate (rather than minimum) temperatures more efficiently minimizes a potential artifact introduced by small dust fragments containing ^{3}He adhered to crystal surfaces (Shuster et al., 2006). Below 600 °C, the samples were heated using a projector lamp heating apparatus in a controlled feedback loop with a thermocouple, as described by Farley et al. (1999). For temperatures between 600 and 1200 °C, we used a 70 W diode laser ($\lambda = 810$ nm) defocused onto the sample in the same thermocouple apparatus, which ultimately enabled complete helium extraction. Both heating procedures were tuned for rapid response and to avoid overshoot of the set-point temperature. Temperature control across this entire range was typically better than ±2 °C.

We used previously described criteria (Shuster et al., 2006) to establish data subsets for Arrhenius regression models for the ^{3}He based experiments: (i) we used the entire set of measured ^{3}He release fractions to calculate D/a^2 values; (ii) we excluded D/a^2 values from regression models for steps when $\Sigma F^3\text{He} \leqslant 0.5\%$ (again, to minimize the influence of small dust fragments which may be present as well as large uncertainties at small yields), and (iii) excluded values for temperatures $\geqslant$280 °C (to avoid the influence of annealing; see below). The only exception was for the synthetic apatites, which did not yield appreciable amounts of helium until well above 300 °C. Step numbers included in these regressions are indicated in bold in Table EA1.

2.4.2. Heating schedule and regression criteria for annealing experiments

For aliquots annealed at temperatures above 250 °C, the heating schedule started at temperatures at least 10 degrees lower than the initial annealing temperature so as to minimize further annealing. It then included a series of retrograde steps, followed by prograde steps typically up to 400 °C. Starting with a retrograde series was adopted to minimize the transient artifact known to occur when temperatures are dropped by a large amount between subsequent diffusion steps (Farley, 2000). For the experiments where the initial temperature of annealing was <250 °C, only the prograde schedule was used. All of these experiments were performed with the projector lamp apparatus described in Section 2.4.1. These experiments usually did not degas the aliquot entirely, so the final yield necessary for diffusion coefficient calculations was obtained either by a total fusion step in a resistance furnace (chips), or by calculation based on the mass of the sample and several determinations of the concentration of He in Dur-B (8.2 nmol/g).

Arrhenius parameters were determined for each aliquot using all data points measured at temperatures <280 °C (at which point further annealing seems likely based on fission track experiments (e.g., Ketcham et al., 2007). In some cases the first steps after annealing were isothermal, in which case only the last of the isothermal measurements was included in the regression (it would make no difference if all isothermal points were included).

3. RESULTS

3.1. Neutron irradiation diffusion experiments

Results of the neutron irradiation and helium diffusion experiments are summarized in Table 1 and the correspond-

ing Arrhenius plots for the six sets of experiments are shown in Fig. 2 and Fig. EA1 in the electronic annex. Primary data for all experiments are tabulated in Table EA1. For all samples, He diffusion coefficients define highly linear Arrhenius arrays at temperatures <280 °C (e.g., Fig. 2). Exposure to a 1 MeV equivalent neutron fluence of 2.3×10^{16} n/cm^2 caused no noticeable change in helium diffusion kinetics in any of the six samples. However, exposing each to a fluence of $2.0–2.7 \times 10^{18}$ n/cm^2 caused increases in both the activation energy (E_a) and in $\ln(D_o/a^2)$, by as much as ~25 kJ/mol and 6.4 $\ln(s^{-1})$, respectively. For example, E_a ranges from 139 kJ/mol in an untreated aliquot of Durango apatite to >161 kJ/mol in those exposed to 90 h of neutron irradiation. In effect, the data arrays in the Arrhenius plots rotate clockwise at temperatures below 550 °C.

Because the two diffusion parameters are so strongly correlated (Fig. 3), for discussion of our observations it makes sense to combine them into a single parameter, specifically the closure temperature. As shown in Fig. 3, the observed array of diffusion parameters cuts obliquely across contours of closure temperature, with higher values of E_a and $\ln(D_o/a^2)$ associated with higher T_c. This indicates that the positive changes in E_a due to radiation exposure are the dominant control on low-temperature retentivity. The radiation resulted in lower values of D/a^2 at lowest temperatures and diffusion kinetics with stronger temperature sensitivity. The resulting closure temperatures increased by 16 to 27 °C after irradiation. Changes in T_c (ΔT_c) negatively scale with the T_c prior to irradiation, indicating that apatites with higher initial T_c were less perturbed by the neutron irradiation than samples with lower initial T_c.

3.2. Thermal annealing diffusion experiments

Complete stepped-heating data for the annealing experiments are compiled in Table EA2 and the segments used for computation of Arrhenius parameters plotted in Supplementary Fig. EA2. Typical results are shown in Fig. 2c. All aliquots yielded highly linear Arrhenius arrays including both the retrograde and the prograde sequences. Both the slope and the intercept of the He diffusion arrays vary among the aliquots (Table 2). For example, the activation energy (E_a) ranges from 139 kJ/mol in an untreated aliquot (identical to previous results (Farley, 2000)) to <100 kJ/mol in those exposed to the most intense annealing conditions. For a given annealing duration, both activation energy and D_o/a^2 generally decrease with temperature and, as with the neutron irradiation experiments, there is a strong correlation between the two Arrhenius parameters (Fig. 3). Table 2 shows that T_c of the variably annealed Durango aliquots ranges from −2 to 78 °C.

4. DISCUSSION

4.1. Relating neutron damage to natural alpha damage

In our previous work, we considered the radiogenic ^{4}He concentration ([^{4}He]) to be a proxy for the volume fraction of naturally occurring radiation damage within each sample today. While [^{4}He] is an easily measurable proxy for radiation damage, it is not ideal for identifying the fundamental controls on helium diffusion. This is because correlations between He diffusivity and ^{4}He might arise from concentration-dependent diffusion rather than radiation damage control, and because radiation damage accumulation (and annealing) in general will not correlate perfectly with the accumulation of alpha particles. Here we improve on the [^{4}He] proxy by developing an alternative indicator of radiation damage. This transformation requires a relationship between the crystal damage caused by neutron irradiation and an equivalent amount of damage caused by natural alpha decay. To make the transformation, we start by assuming that the amount of crystal damage caused by a particular event is proportional to the total amount of ionizing kinetic energy released into the matter of interest (or *kerma* (ASTM, 1994)). With a scaling relationship between the kerma due to neutron irradiation and the kerma due to alpha decay, we can inter-relate the amount of damage caused by each process. This approach assumes that the atomic displacements caused by neutrons are similar to those caused by alpha decay. In addition, we assume that damage associated with induced fission of ^{235}U is insignificant, particularly because we used Cd shielding which minimizes the thermal neutron flux. We will focus our discussion on kerma, since it is a quantity that is more easily related to radiation damage than is [^{4}He], and allows us to compare damage caused by different types of radiation.

The kerma for a particular neutron irradiation is a function of the energy spectrum and the amount of time a sample resided within a specific nuclear reactor. The energy spectrum within the CLICIT facility at OSU is well-known at the location of our samples, shown in Fig. EA3. Using the American Society for Testing and Materials (ASTM) standard practice for characterizing neutron energy fluence spectra for radiation hardness testing (ASTM, 1994), the 1 MeV equivalent monoenergetic damage function for silicon has been calibrated for the OSU CLICIT facility by S. Reese (personal communication), equaling 6.3×10^9 n/kW s cm^2. From this calibration, we can estimate the 1 MeV equivalent neutron fluence ($\Phi_{eq,\ 1MeV,\ Si}$) for each experimental condition (note the OSU reactor was operated at 1 MW for our experiments). Since the kerma for silicon has also been quantified (Nameson et al., 1972), we can simply relate $\Phi_{eq,\ 1MeV,\ Si}$ to the Si kerma by using the ASTM standard 1 MeV neutron displacement kerma factor ($K_{D,\ 1MeV,\ Si}$) of 95 ± 4 MeV mb (ASTM, 1994) and the mean atomic mass of Si as shown in Fig. 4a.

The kerma for α-decays along the U- and Th-decay chains is given by the mean Q-value for the set of α-decays (~5.7 MeV/α-decay). By assuming quantitative retention of ^{4}He, which will be true at temperatures below ~40 °C, we can relate the kerma resulting from α-decay to an equivalent radiogenic ^{4}He concentration in apatite ("alpha equivalent units", or [^{4}He]$_{eq}$) (Fig. 4a). Note that the reaction Q-value carries all available energy for causing crystal damage, including both the kinetic energy of the α-particle and the recoiled parent nucleus. Here, we ignore the small amount of total kerma due to naturally occurring but relatively infrequent spontaneous ^{238}U fission events.

Table 1
Neutron irradiation experiments.

Sample	$[^4He]_o$ (nmol/g)	Reactor time (h)	J	1-MeV eq. neutron fluence (10^{16} n/cm^2)	$[^4He]_{eq}$ (nmol/g)	$[^3He]$ (nmol/g)	$[^4He]_{tot}$ (nmol/g)	E_a (kJ/mol)	(+/−) (kJ/mol)	$\ln(D_o/a^2)$ $\ln(s^{-1})$	(+/−) $\ln(s^{-1})$	T_c (°C)	(+/−) (°C)
WSAp_A	0.000	0	0.00000	0.0	0.00	0.0037	0.037	132	0.8	5.66	0.14	117.2	0.9
WSAp_B	0.000	1	0.00027	2.3	0.13	0.0017	0.038	133	1.1	5.82	0.21	118.4	1.3
WSAp_D	0.000	10	0.00260	26.8	1.56	0.0042	0.410	132	1.8	4.77	0.32	126.5	2.2
WSAp_C	0.000	90	0.02343	204.1	11.86	0.0036	2.150	149	0.6	8.04	0.10	143.8	0.6
DAp_A	8.200	0	0.00000	0.0	8.20	0.0023	8.200	139	2.2	13.54	0.55	73.1	1.5
DAp_B	8.200	1	0.00027	2.3	8.33	0.0022	7.500	138	0.9	13.38	0.21	72.1	1.0
DAp_C	8.200	90	0.02343	204.1	20.06	0.0022	8.633	161	2.0	19.25	0.50	86.7	1.1
DAp_D	8.200	90	0.02343	204.1	20.06	0.0022	8.824	164	2.1	19.92	0.51	87.8	1.1
01mr59[a]	0.500	0	0.00000	0.0	0.50	0.0025	0.500	121	1.5	10.50	0.40	49.2	6.6
01mr59_A	0.500	1	0.00027	2.3	0.63	0.0019	0.793	123	1.2	11.73	0.29	44.5	1.2
01mr59_B	0.500	90	0.02343	204.1	12.36	0.0022	3.016	134	2.1	11.55	0.53	74.5	1.5
01mr59_C	0.500	90	0.02343	204.1	12.36	0.0022	2.926	135	1.0	12.79	0.25	69.6	0.7
DYJS5[b]	0.300	0	0.00000	0.0	0.30	0.0020	0.300	122	1.2	10.50	0.30	49.9	5.1
DYJS5_A	0.300	90	0.02343	204.1	12.16	0.0022	2.545	128	2.1	10.32	0.52	67.5	1.6
CJ50[b]	0.010	0	0.00000	0.0	0.01	0.0020	0.010	121	0.9	10.20	0.20	49.4	3.7
CJ50_A	0.010	100	0.02645	267.8	15.56	0.0026	1.668	136	0.8	10.86	0.16	85.0	0.8
00mr18[b]	0.040	0	0.00000	0.0	0.04	0.0020	0.040	149	2.7	21.40	0.70	47.2	9.6
00mr18_A	0.040	100	0.02645	267.8	15.60	0.0024	1.443	165	4.7	21.15	1.19	81.9	2.4

$[^4He]_o$ is the initial radiogenic ^4He concentration; J is the neutron irradiation parameter (Grasty and Mitchell, 1966); the 1-MeV equivalent neutron fluence is estimated from empirical calibration as described in the text; $[^4He]_{eq}$ is the alpha equivalent concentration for each irradiation estimated from Fig. 4 and $[^4He]_o$; $[^3He]$ and $[^4He]_{tot}$ are the measured helium isotope concentrations; E_a is the activation energy for helium diffusion; $\ln(D_o/a^2)$ is the natural log of the frequency factor, and T_c is the helium closure temperature calculated for $dT/dt = 10$ °C/Ma. nmol $= 10^{-9}$ mol.

[a] Shuster et al. (2005).

[b] Shuster et al. (2006).

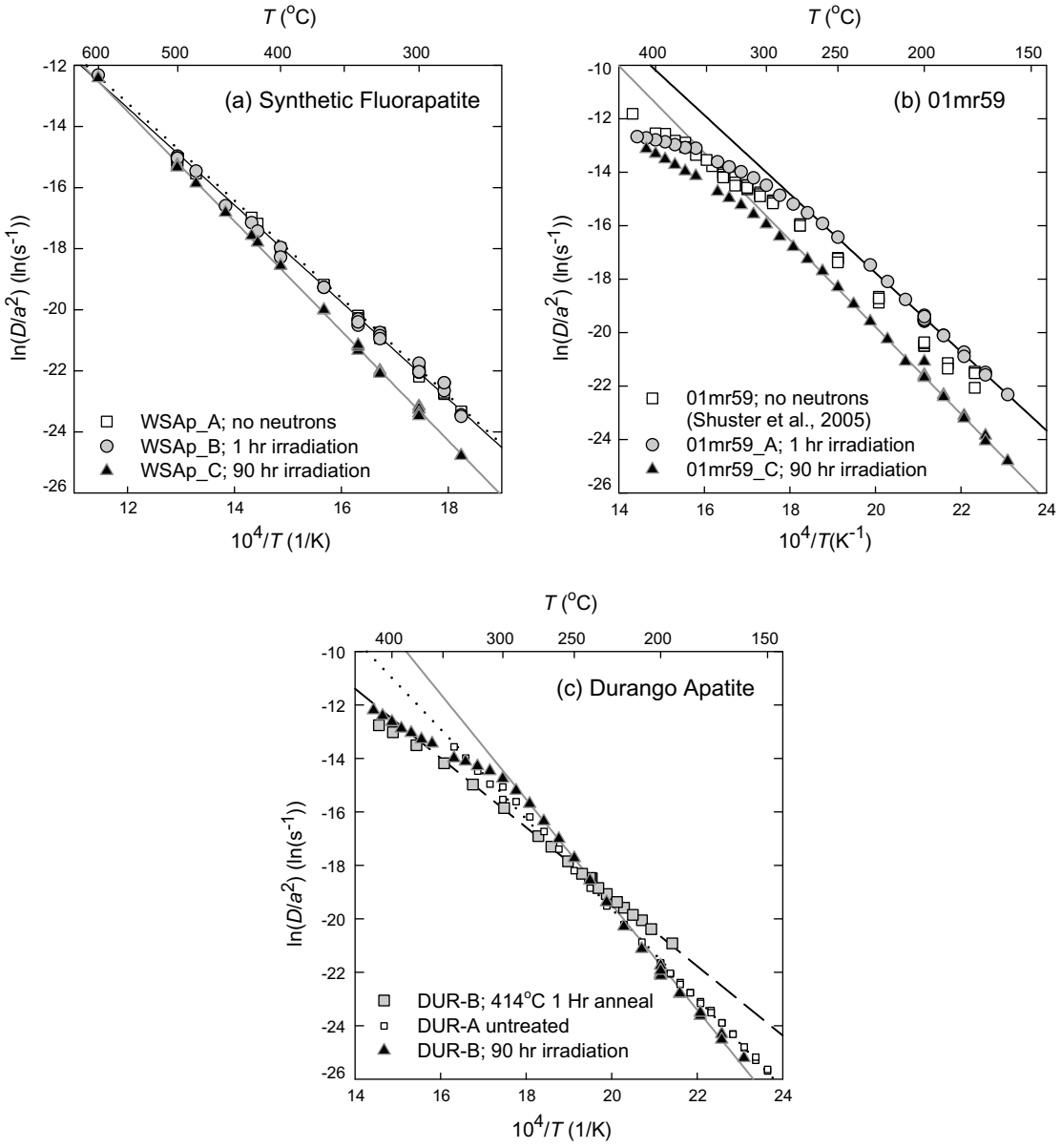

Fig. 2. Example He diffusion Arrhenius plots for (a) synthetic apatite WSAp before and after neutron irradiation, (b) 01MR59 before and after neutron irradiation, and (c) Durango apatite showing results from untreated DUR-A (Farley, 2000), and DUR-B subjected to 90 h of neutron irradiation and DUR-B subjected to 1 h of annealing at 414 °C (gray squares). Lines are the helium diffusion kinetics determined by linear regression to subset arrays selected using the criteria discussed in the main text and indicated in Tables EA1 and EA2. Open squares are the control experiments without any time in the nuclear reactor or thermal annealing, circles are 1 h irradiations and diamonds are 90 h irradiations. In all cases neutron irradiation causes Arrhenius arrays to rotate clockwise, yielding higher closure temperatures. In contrast, annealing does just the opposite. Arrhenius plots for all samples are including in the electronic annex.

By assuming that the kerma for silicon during the time in the OSU reactor is approximately equal to the kerma for apatite for the same irradiation conditions, we can set the two functions in Fig. 4a equal to one another to derive a relationship between $\Phi_{eq,\ 1MeV,\ Si}$ and $[^4He]_{eq}$. This allows us to semi-quantitatively express the expected crystal damage caused by neutron irradiation (most likely due to nuclear scattering reactions) in terms of alpha equivalent units and to compare these results with the natural variations observed by Shuster et al. (2006). Although this relationship is clearly an oversimplification, we discuss below and demonstrate in Fig. 1 that the relationship in Fig. 4b appears to be valid. The relationship also allows us to express the previous results of Shuster et al. (2006) in terms of kerma (e.g., Fig. 7).

4.2. Experimental complications

The relatively small amount of kerma introduced by our proton irradiation (Summers et al., 1993), as well as

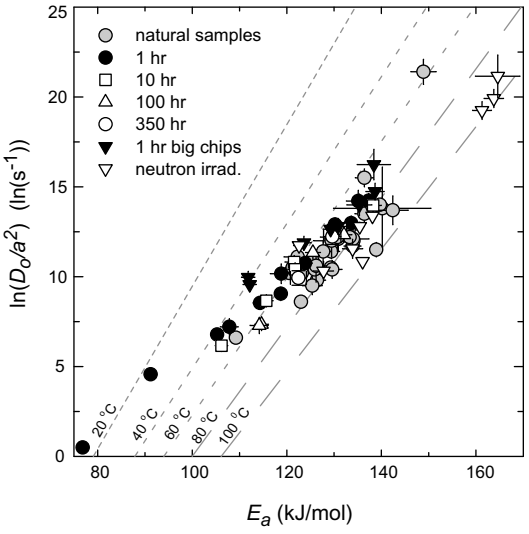

Fig. 3. He diffusion parameters $\ln(D_o/a^2)$ and E_a for natural apatites (Shuster et al., 2006), for neutron irradiated natural apatites, and for the annealed Durango apatite aliquots. The specified number of hours corresponds to the Durango apatite annealing experiments conducted at different temperatures, as shown in Figs. 4 and 5. All samples define a roughly linear trajectory on this figure, which we associate with the effects of radiation damage. Increasing damage moves samples to the northeast, annealing moves them to the southwest. Also shown and labeled are contours of closure temperature (calculated for $dT/dt = 10$ °C/Ma). Note that the sample array crosses closure temperature contours at an oblique angle, showing how increasing or decreasing amounts of radiation damage propagates into changes in closure temperature.

thermal annealing during the neutron irradiations may complicate our ability to relate neutron-induced damage to the observations of Shuster et al. (2006). However, due to the log-linear relationship between kerma and T_c, each introduces only a small bias in Fig. 1. The kerma introduced during the 8 h of proton irradiation is only $\sim 10^{14}$ MeV/g, compared with $\sim 10^{16}$ or more in most natural samples. We therefore expect proton-induced damage to be insignificant relative to a sample's initial or neutron-induced damage except for those samples containing very low amounts of initial kerma (particularly the synthetic apatite, CJ50 and 00mr18). Comparison of Fig. 1 with Fig. 7 (which includes kerma due to proton irradiation), reveals only a slight difference in the location of these samples. However, we now believe that the trapping model as calibrated in Shuster et al. (2006) (Fig. 1) may be biased towards high T_c for kerma values below $\sim 10^{14}$ MeV/g. Since T_c is expected to rapidly increase with relatively small amounts of kerma, under most circumstances this is a minor artifact (see below).

In addition to causing crystal damage, the neutron irradiations caused two bi-products during irradiation: ^{4}He (primarily from (n, α) reactions while in the reactor) and heat. Although the latter introduces the potential for a small amount of bias in Fig. 1 due to concurrent annealing during neutron irradiations, we show that these complications also provide an interesting way to monitor the average temperature of a sample while in the reactor. As discussed in the electronic annex, we can estimate the ^{4}He production rate in our samples from known reaction cross sections on ^{40}Ca, ^{16}O, and ^{19}F. Since we know the total amount of time spent in the reactor, we can use the measured diffusion kinetics both before and after irradiation to solve for the mean temperature of the sample using ^{4}He/^{3}He thermochronometry (Shuster and Farley, 2004). In effect, this is a controlled experiment involving simultaneous in-growth and diffusion of ^{4}He. Fig. EA5 shows the result of this analysis, clearly indicating that the samples reached a mean temperature of ~260 °C. This temperature corroborates a previous, independent measurement of maximum temperature (270 °C) made in the same facility using a thermocouple embedded in an aluminum block. This temperature has important implications for ^{40}Ar/^{39}Ar geochronology, particularly when conducted on K bearing glass which is likely to diffuse Ar at ~260 °C during irradiation (Shuster et al., 2005).

Although the small amount of concurrent annealing expected at this temperature in the reactor will cause the samples to plot at higher kerma in Figs. 1 and 7 than is appropriate, the shift is relatively small given the logarithmic x-axis.

4.3. The influence of neutron irradiation on synthetic apatite

The trapping model of Shuster et al. (2006) predicts that proton-irradiated apatite otherwise devoid of radiation damage should have diffusion kinetics defined by the two parameters: $E_a = 120$ kJ/mol and $D_o/a^2 = 1.58 \times 10^4$ s^{-1}, corresponding to $T_c \sim 52$ °C. Our experiments on synthetic fluorapatite were designed, in part, to test this prediction. Assuming that the synthetic apatite has exactly the same properties as natural apatite, we expected T_c to be at or below the least retentive apatites observed in Shuster et al. (2006). However, this is not observed. Instead, even in the untreated specimen we found helium diffusion kinetics approximately equal to the most retentive natural apatite, or ~117 °C (Figs. 1 and 2a). We do not understand why the synthetic apatite is so He retentive, but we suspect it is related to large differences in defect density between the synthetic and natural specimens.

Another striking feature of the synthetic apatite Arrhenius plot is a lack of curvature between 270 and 900 °C, a linearity that is almost never observed in natural apatites (See Fig. EA1 and Farley, 2000; Shuster et al., 2004, 2005, 2006). While these discrepancies make the synthetic apatite an imperfect analog system, the sample's response to neutron irradiation is remarkably similar to natural samples.

The 10 and 90 h neutron irradiations of the synthetic apatite caused E_a and D_o/a^2 to increase dramatically (Table 1). The resulting change in T_c from 90 h of neutron irradiation ($\Delta T_c \sim +27$ °C) spans most of the observed range in T_c for natural apatites (Fig. 1). When plotted against alpha equivalent units ($[^4\text{He}]_{eq}$) or kerma, we find the relative increases in T_c are in good agreement with the trapping model of Shuster et al. (2006) when shifted upwards to have a base $T_c \sim 117$ °C (gray curve in Fig. 1).

Table 2
Thermal annealing experiments.

Aliquot	Annealing T (°C)	Annealing time (h)	E_a (kJ/mol)	(+/−) (kJ/mol)	$\ln(D_o/a^2)$ $\ln(s^{-1})$	(+/−) $\ln(s^{-1})$	T_c (°C)	(+/−) (°C)	Fraction lost in annealing step
Shards									
No pretreatment			141	1.7	14.23	0.40	72.5	1.3	
H1-T75	75	1	140	2.5	14.21	0.60	71.2	1.9	1.00E−04
H1-T300	300	1	137	1.7	12.98	0.40	72.0	1.3	7.30E−02
H1-T325	325	1	133	1.6	12.90	0.39	63.9	1.3	1.14E−01
H1-T350	350	1	127	1.5	10.75	0.37	62.4	1.3	9.50E−02
H1-T354	354	1	123	2.3	10.17	0.55	57.4	2.1	1.50E−01
H1-T365	365	1	121	1.2	9.05	0.38	59.4	0.4	1.80E−01
H1-T375	375	1	117	1.5	8.54	0.35	52.4	1.2	1.99E−01
H1-T397	397	1	112	1.9	7.21	0.46	46.6	1.7	2.14E−01
H1-T414	414	1	108	1.3	6.78	0.32	39.2	1.1	3.13E−01
H1-T450	450	1	94	1.3	4.57	0.32	14.1	1.1	8.70E−01
H1-T500	500	1	79	1.3	0.50	0.32	-2.1	1.2	9.40E−01
H10-T250	250	10	142	1.7	13.97	0.42	76.9	1.4	5.60E−02
H10-T275	275	10	135	1.7	12.67	0.40	68.8	1.3	1.14E−01
H10-T300	300	10	125	2.0	10.82	0.37	58.0	2.3	2.27E−01
H10-T315	315	10	125	1.5	10.41	0.37	59.2	1.3	2.75E−01
H10-T330	330	10	119	1.5	8.66	0.35	55.1	1.2	2.59E−01
H10-T345	345	10	109	1.3	6.16	0.32	46.3	1.1	2.79E−01
H100-T250	250	100	135	1.7	12.33	0.40	72.8	1.4	8.90E−02
H100-T275	275	100	129	1.6	11.35	0.38	62.7	1.3	3.27E−01
H100-T300	300	100	118	1.5	7.35	0.35	62.0	1.3	2.88E−01
H100-T325	325	100	118	1.9	7.29	0.46	63.7	1.7	7.70E−01
H350-T250	250	350	133	1.8	12.23	0.44	68.1	1.5	2.95E−01
H350-T270	270	350	126	1.7	9.93	0.41	65.4	1.5	3.59E−01
Chips (diffusivities recomputed to r = 85 μm)									
No pretreatment			141	2.7	14.00	0.60	74.1	2.3	
BH1-T150	150	1	145	3.5	16.24	0.85	70.6	2.7	1.67E−05
BH1-T250	250	1	143	2.0	14.74	0.47	73.7	1.5	1.20E−03
BH1-T325	325	1	135	1.9	12.80	0.45	67.7	1.6	1.00E−02
BH1-T350	350	1	133	1.6	12.65	0.39	63.4	1.3	2.00E−02
BH1-T375	375	1	127	1.5	11.89	0.37	53.9	1.2	3.20E−02
BH1-T391	391	1	115	1.4	9.97	0.33	35.7	1.1	5.40E−02
BH1-T415	415	1	115	1.4	9.57	0.33	39.2	1.1	5.90E−02

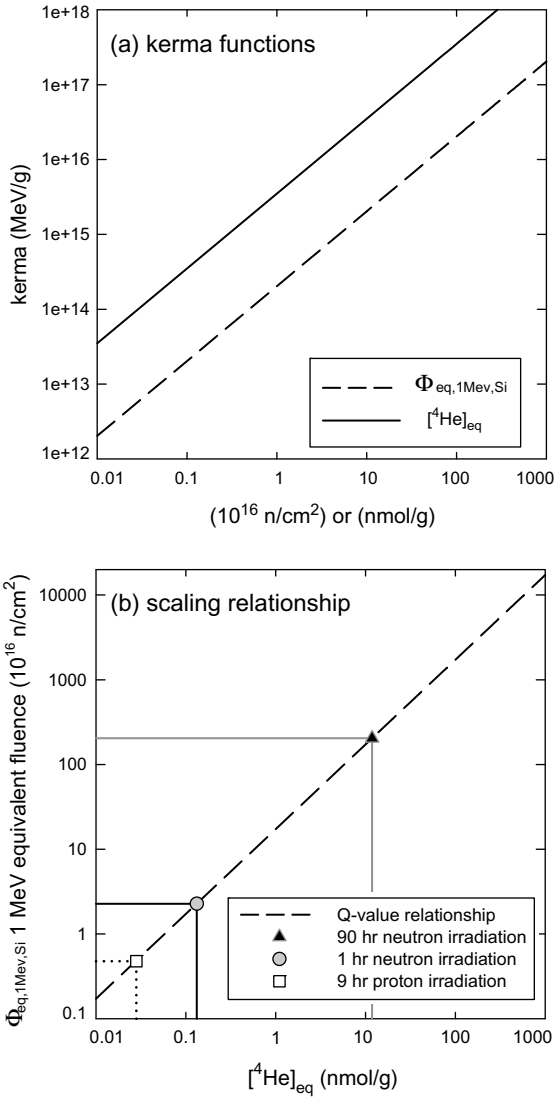

Fig. 4. Kerma scaling. (a) The relationships between the total kinetic energy released into matter (kerma) and (i) the 1 MeV equivalent neutron fluence ($\Phi_{eq,\ 1\ MeV,\ Si}$) and (ii) the alpha equivalent units due to U- and Th-decay series assuming quantitative ^{4}He retention ($[^4He]_{eq}$). (b) The scaling relationship between $\Phi_{eq,\ 1MeV,\ Si}$ and $[^4He]_{eq}$ derived by setting the two lines equal to one another in (a). Shown are the equivalent ^{4}He concentrations for 90 and 1 h in the OSU nuclear reactor, and 9 h of irradiation in the 200 MeV proton beam at the Francis H. Burr Proton Therapy Center.

This agreement corroborates the parameters $E_t = 29$ kJ/mol and $\psi = 1.26 \times 10^{-4}$ g/nmol of Shuster et al. (2006) and also indicates that the kerma scaling relationship in Fig. 4 is not grossly inaccurate.

4.4. The influence of neutron irradiation on natural apatite

Just like in the synthetic apatite, in all five natural apatites, exposure to increasing amounts of neutron irradiation caused E_a, D_o/a^2 and the He closure temperature to increase (Table 1). The fact that ΔT_c negatively scales with initial T_c indicates that the neutron-induced damage was additive to the natural damage, but in a logarithmic sense. This agrees with the log-linear relationship observed in natural samples and predicted by the trapping model (Shuster et al., 2006). This is most clearly observed in Fig. 1. For example, samples CJ50 and 00mr18, which contain a small amount of initial kerma and a $T_c \sim 50$ °C, end up with $T_c \sim 82$ and 85 °C, (or differences of +32 and +35 °C). On the other hand, Durango, which initially contains a far larger amount of kerma and initial $T_c = 72$ °C is only perturbed by +14 °C. When plotted against $[^4He]_{eq}$ or kerma, all five samples plot very close to the closure temperatures observed for natural apatites with an equivalent amount of damage and close to that predicted by the trapping model.

The main observation of Shuster et al. (2006) was a correlation between T_c and log($[^4He]$) in a suite of natural apatites. While radiation damage trapping of ^{4}He is a reasonable explanation for this correlation, the possibility of concentration-dependent-diffusion could not be ruled out. The neutron irradiation experiments described here provide a test between these possibilities, as do the annealing experiments (see Section 4.5). Only a small fraction of neutrons produce ^{4}He (see electronic annex), but almost all participate in damage production. In contrast, in the case of α-decay, the production of radiation damage is genetically tied one-to-one with ^{4}He production. Thus, the neutron irradiated samples accumulate radiation damage faster than ^{4}He. For example, the measured ^{4}He concentrations following 90 and 100 h neutron irradiations ($[^4He]_{tot}$ in Table 1) are typically ~1 order of magnitude lower than the alpha equivalent units of radiation damage.

Fig. 1 shows that the response of He diffusion to neutron irradiation is correlated with damage accumulation rather than ^{4}He accumulation. For example, the 100 h experiments for samples CJ50 and 00mr18 plot as predicted from their increased kerma (Fig. 1), yet if they were plotted against $[^4He]_{tot}$, they would plot significantly higher in T_c than the main population. The distinction between radiation damage and $[^4He]$ is perhaps most clearly seen in the Durango apatite results. The in-reactor ^{4}He production and diffusive loss were fortuitously balanced such that the final ^{4}He concentration after neutron irradiation ($[^4He]_{tot} \sim 8.7$ nmol/g) was approximately equal to the initial ^{4}He concentration (~8.2 nmol/g). Despite nearly equivalent $[^4He]$, the T_c after 90 h of neutron irradiation was higher by ~15 °C. This clearly indicates that a variable other than $[^4He]$ is controlling helium retentivity in the sample. When plotted against $[^4He]_{eq}$ or kerma (Fig. 1), the increase in T_c is close to that predicted by the trapping model, again strongly indicating that radiation damage is the controlling variable.

4.5. Kerma as a predictive variable

When scaled to the total kinetic energy available for displacing atoms, the neutron irradiations caused changes in helium diffusion kinetics that are in good agreement with the observed range in natural apatites and the model of Shuster et al. (2006). Because we did not induce significant

quantities of fission events (due to the Cd shielding and comparatively low natural abundances of fissionable ^{235}U), this suggests that helium diffusivity in natural samples is also controlled by kerma, which is dominated by alpha decays rather than fission track events. For example, since spontaneous fission amounts to such a small amount of the natural kerma budget, the influence of fission would hardly be observable in Fig. 7. Although the energy released by a spontaneous fission event can be ~35 times greater than an alpha decay, low event probability causes the cumulative ratio of fission kerma to alpha kerma to be $<10^{-5}$. These experiments suggest but do not prove that alpha decay, rather than fission, is the dominant source of radiation damage that controls He diffusion.

For purposes of an empirically calibrated diffusion model extrapolated over geologic time, these distinctions may not be essential. This is because in most apatites, alpha decay is dominated by ^{238}U. Since this is the isotope that also fissions spontaneously, alpha damage and fission damage accumulate in lock step. However, for rare apatites with very high Th/U ratios, the ratio of fissions to alpha decays will be lower. In future work this distinction may provide a way to identify the relative impact of alpha decay and fission decay on He diffusion kinetics.

4.6. The influence of thermal annealing on natural apatite

Our data on the annealed aliquots confirms that heating to temperatures above ~270 °C causes an irreversible change in the He diffusion behavior in Durango apatite (Farley, 2000). In effect the diffusion array rotates counterclockwise, yielding lower values for E_a, $\ln(D_o/a^2)$, and T_c. The magnitude of the effect increases with both temperature and time. The observed ranges in E_a, $\ln(D_o/a^2)$, and T_c in the variably annealed aliquots encompass almost the entire range documented by Shuster et al. (2006) in natural apatites. Furthermore, as shown in Fig. 3 the strong correlation between E_a and $\ln(D_o/a^2)$ observed in the annealing experiments is identical to correlations found in both the untreated natural samples and the natural samples subjected to neutron irradiation. These similarities seem unlikely to be coincidental and instead suggest that the annealing step reverses the changes in helium diffusion that are correlated with increasing ^{4}He in untreated apatites and with increasing neutron fluence in the irradiated apatites.

As shown in Fig. 5a, for a given duration of annealing there is a negative correlation between T_c and [^{4}He] remaining after the annealing step, as might be expected for concentration-dependent diffusion. However, different durations of annealing yield very different arrays on the plot, and, most notably, the coarse chips suffered relatively little fractional ^{4}He loss but closure temperature reductions almost identical to those in the shard experiments. These observations along with the neutron irradiation experiments (Section 4.4) eliminate the possibility that ^{4}He concentration itself is controlling diffusivity.

Fig. 5b highlights the role of annealing temperature on the resulting He diffusion kinetics. There is essentially no change in T_c for annealing steps below 290 °C, but above 290 °C T_c drops rapidly. For a given annealing temperature, the longer the duration of the annealing step the greater the reduction in T_c. This pattern is consistent with a thermally activated process: both temperature and time matter. The most straightforward explanation for these data is that radiation damage naturally present in Durango is annealing, and the annealing is reducing the abundance and/or size of radiation damage traps (Shuster et al., 2006) that impede helium migration. If so, Fig. 5b carries information on the kinetics of annealing which could be transformed into a predictive kinetic model for He diffusion. However, rather than develop a completely new model

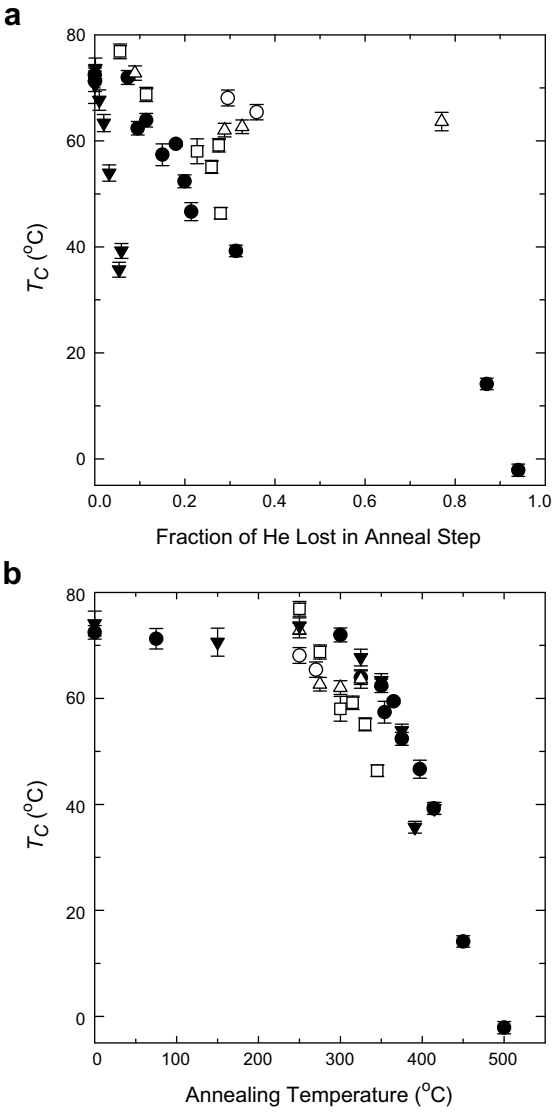

Fig. 5. The He closure temperature (T_c) in variably annealed DUR-B against (a) fraction of ^{4}He remaining in the sample after the annealing step, and (b) the holding temperature for the annealing step. This figure shows that the ^{4}He concentration remaining in the sample is not a good predictor of the closure temperature after annealing. However, it is clear that higher temperatures and longer durations of annealing lead to systematically lower closure temperatures beginning above about 290 °C. Symbols are the same as in Fig. 3.

it seems sensible to examine whether existing damage annealing models can account for the observed patterns.

The annealing of fission tracks in Durango apatite has been the focus of many years of research (Green, 1988; Carlson et al., 1999; Ravenhurst et al., 2003; Ketcham, 2005). While the vast majority of the radiation damage in this sample must be derived from α-recoil of parent nuclei rather than fission tracks, inter-comparison of these datasets proves useful. Based on the temperature and time of the annealing experiments, we computed the expected fission track length (normalized to the initial length) according to the Durango fanning curvilinear model of Ketcham et al. (2007). Note that this model yields lengths that decrease with temperature and time until the proportional length reduction, normalized for track angle, is ~0.5, at which point further annealing causes total disappearance of etched tracks. The computed track length in our aliquots range from unity to total disappearance.

As shown in Fig. 6, there is a strong linear correlation between T_c and predicted track length: reduction in normalized length from unity to 0.5 is associated with a T_c reduction of ~25 °C. An important observation from this figure is that all experiments, regardless of temperature and time, collapse on to a single correlation array. This is critical evidence that this fission track annealing model can quantitatively account for changes in He diffusivity in Durango apatite despite the fact that the model is designed to predict fission track rather than alpha recoil damage annealing.

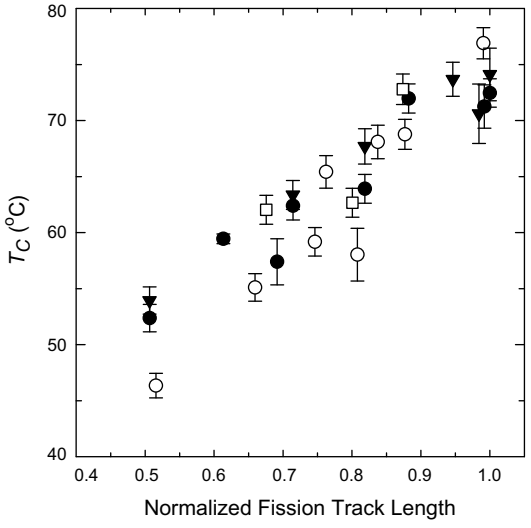

Fig. 6. The He closure temperature (T_c) as a function of the normalized fission track length predicted to remain in each sample after the annealing step. Lengths were computed using the Durango kinetic model of Ketcham et al. (2007) and were normalized to the initial length. The roughly linear correlation between helium closure temperature and the degree of fission track annealing independent of annealing conditions strongly suggests that (i) the He is responding to the annealing of radiation damage in the apatite, and (ii) the fission track annealing model of Ketcham et al. (2007) provides a fairly accurate kinetic description of the annealing process to which He is sensitive.

When normalized fission track lengths drop below 0.5, any further annealing causes the tracks to disappear completely (e.g., Carlson et al., 1999). However, He diffusion kinetics demand continued structural modification beyond this point. In the most extreme case, when heated to 500 °C for 1 h, T_c drops to the remarkably low value of −2 °C—a drop of ~45 °C after all etchable tracks have disappeared. One possible explanation for this paradox is that the fission tracks simply become unetchable before all associated damage is completely erased. In this case the tracks may still be present and undergoing further annealing, but the mechanism by which they are revealed fails. Alternatively, fission damage may erase completely before α-recoil damage does. If so, the kinetics of α-recoil and fission damage annealing would have to be quite similar for at least the first 25 °C of T_c reduction (Fig. 6).

Fig. 3 demonstrates a strong similarity in He diffusion parameter behavior among (i) untreated apatites, (ii) samples subjected to neutron irradiation; and (iii) the Durango aliquots which are variably annealed. In the cases (i) and (ii), increasing radiation damage causes apatites to move to higher E_a, $\ln(D_o/a^2)$ and therefore higher T_c. Annealing drives apatites in exactly the reverse direction. Fig. 7 shows this concept in a different way. Rather than plot T_c against the [^{4}He] proxy for radiation damage as done previously (Shuster et al., 2006), here T_c is plotted against kerma, this time including the kerma from proton irradiation. The vectors indicate the direction in which damage accumulation on the one hand and damage annealing on the other drive a sample. While it is straightforward to plot the natural samples and the neutron irradiated samples on this figure because their kerma can be estimated, we do not know how to relate fission track length reduction to erasure of

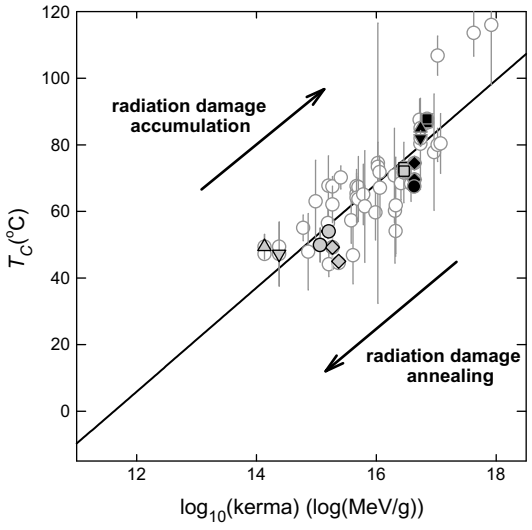

Fig. 7. The competing influence of radiation damage accumulation and annealing on helium diffusion kinetics. The points are those shown in Fig. 1 scaled onto the kerma axis according to Fig. 3 including a small amount of kerma from the proton irradiations. Arrows indicate the sense of influence of damage accumulation and annealing. The line is a linear regression through the data extrapolated to low values of kerma.

the effects of kerma. Thus, while we can plot the single untreated Durango apatite point on this figure, it is impossible to plot the annealing experiments.

However, a rough estimate of the relationship between kerma and fission track length reduction can be obtained by combining Figs. 6 and 7. A regression line through the data in Fig. 7 shows that T_c increases by about 16 °C for each log unit of kerma added. Combined with the slope from Fig. 6, this correlation suggests that a 50% reduction in track length associated with a 25 °C drop in T_c, is equivalent in magnitude but opposite in sign to the effects of adding 1.6 log units of kerma. Thus, the 25 °C reduction in T_c associated with track length reduction from unity to 0.5 corresponds to elimination of about 97% of the accumulated damage to which He diffusion is sensitive. Using the same logic, the reduction of T_c to −2 °C in the most annealed Durango aliquot corresponds to elimination of all but ~40 ppm of the original damage. It seems likely that at some point He diffusion is no longer influenced by structural imperfections such that further annealing ceases to lower T_c, but we have not yet reached that point in our experiments.

5. CONCLUSIONS

These experiments unambiguously demonstrate that the amount of radiation damage in an apatite crystal has a strong influence on its helium diffusion kinetics. In what appears to be a reversible process, exposing samples to increasing levels of radiation causes the closure temperature to increase, whereas thermal annealing above 290 °C for 1 h causes it to decrease. In the controlled irradiation experiments, the observed log-linear relationship between kerma and T_c corroborates the trapping model of Shuster et al. (2006) originally documented using natural samples. The thermal annealing results provide a basis on which to develop a quantitative model incorporating both damage production and annealing kinetics as controls on helium diffusion kinetics. A refined model for this entire process on arbitrary time–temperature paths, and its consequences for He diffusion in apatite and for (U–Th)/He cooling ages, will be discussed in a subsequent publication.

ACKNOWLEDGEMENTS

We thank D. Cherniak for providing the synthetic apatite sample, R. Ketcham for guidance on fission track annealing, R. Ewing and R. Fleming for helpful discussion about kerma, S. Reese for access to the neutron energy spectrum and the $\Phi_{eq,\ 1MeV,\ Si}$ calibration for the CLICIT, T. Becker for help with neutron irradiations, and P. Reiners and two anonymous referees for helpful reviews. This work was supported by NSF Grants EAR-0738474 to DLS and EAR-0738627 to KAF and the Ann and Gordon Getty Foundation.

APPENDIX A. SUPPLEMENTARY DATA

Supplementary data associated with this article can be found, in the online version, at doi:10.1016/j.gca.2008.10.013.

REFERENCES

ASTM (1994) ASTM Subcommittee E10-07 on Radiation Dosimetry for Radiation Effects on Materials and Devices: Standard Practice for Characterizing Neutron Energy Fluence Spectra in Terms of an Equivalent Monoenergetic Neutron Fluence for Radiation-Hardness Testing for Electronics. **E 772-94**, 1–16.

Carlson W. D., Donelick R. A. and Ketcham R. A. (1999) Variability of apatite fission-track annealing kinetics: I. Experimental results. *Am. Mineral.* **84**(9), 1213–1223.

Cherniak D. J. (2005) Uranium and manganese diffusion in apatite. *Chem. Geol.* **219**(1–4), 297–308.

Crowley P. D., Reiners P. W., Reuter J. M. and Kaye G. D. (2002) Laramide exhumation of the Bighorn Mountains, Wyoming: an apatite (U–Th)/He thermochronology study. *Geology* **30**(1), 27–30.

Ewing R. C., Weber W. J. and Clinard J. F. W. (1995) Radiation effects in nuclear waste forms for high-level radioactive waste. *Prog. Nucl. Energy* **29**(2), 63–127.

Farley K. A. (2000) Helium diffusion from apatite: general behavior as illustrated by Durango fluorapatite. *J. Geophys. Res.* **105**, 2903–2914.

Farley K. A., Reiners P. W. and Nenow V. (1999) An apparatus for high-precision helium diffusion measurements from minerals. *Anal. Chem.* **71**, 2059–2061.

Fechtig H. and Kalbitzer S. (1966) The diffusion of argon in potassium-bearing solids. In *Potassium Argon Dating* (eds. O. A. Schaeffer and J. Zahringer). Springer-Verlag, New York, pp. 68–106.

Flowers R. M., Shuster D. L., Wernicke B. P. and Farley K. A. (2007) Radiation damage control on apatite (U–Th)/He dates from the Grand Canyon region, Colorado Plateau. *Geology* **35**(5), 447–450.

Grasty R. and Mitchell J. (1966) Single sample potassium–argon ages using the Omegatron. *Earth Planet. Sci. Lett.* **1**(3), 121–122.

Green P. F. (1988) The relationship between track shortening and fission-track age reduction in apatite—combined influences of inherent instability, annealing anisotropy, length bias and system calibration. *Earth Planet. Sci. Lett.* **89**(3–4), 335–352.

Green P. F., Crowhurst P. V., Duddy I. R., Japsen T. and Holford S. P. (2006) Conflicting (U–Th)/He and fission track ages in apatite: enhanced He retention, not anomalous annealing behaviour. *Earth Planet. Sci. Lett.* **250**(3–4), 407–427.

Green P. F. and Duddy I. R. (2006) Interpretation of apatite (U–Th)/He ages and fission track ages from cratons. *Earth Planet. Sci. Lett.* **244**(3–4), 541–547.

Hurley P. M. (1952) Alpha ionization damage as a cause of low He ratios. *Trans. Am. Geophys. Union* **33**, 174–183.

Hurley P. M. (1954) The helium age method and the distribution and migration of helium in rocks. In *Nuclear Geology* (ed. H. Faul). John Wiley and Sons, New York, pp. 301–329.

Ketcham R. A. (2005) Forward and inverse modeling of low-temperature thermochronometry data. In *Low-Temperature Thermochronology: Techniques, Interpretations, and Applications*, vol. 58, pp. 275–314.

Ketcham R. A., Carter A., Donelick R. A., Barbarand J. and Hurford A. J. (2007) Improved modeling of fission-track annealing in apatite. *Am. Mineral.* **92**(5–6), 799–810.

Meesters A. G. C. A. and Dunai T. J. (2002) Solving the production-diffusion equation for finite diffusion domains of various shapes. Part II. Application to cases with α-ejection and non-homogeneous distribution of the source. *Chem. Geol.* **186**, 57–73.

Nameson A. L., Wolicki E. A. and Messenger G. C. (1972) Average silicon neutron displacement kerma factor at 1 MeV. *IEEE Trans. Nucl. Sci.* **29**(1), 1018–1020.

Nasdala L., Reiners P. W., Garver J. I., Kennedy A. K., Stern R. A., Balan E. and Wirth R. (2004) Incomplete retention of radiation damage in zircon from Sri Lanka. *Am. Mineral.* **89**(1), 219–231.

Prener J. S. (1967) Growth and crystallographic properties of calcium fluor- and chlorapatite crystals. *J. Electrochem. Soc.* **114**(1), 77.

Ravenhurst C. E., Roden-Tice M. K. and Miller D. S. (2003) Thermal annealing of fission tracks in fluorapatite, chlorapatite, manganoanapatite, and Durango apatite: experimental results. *Can. J. Earth Sci.* **40**(7), 995–1007.

Shuster D. L., Ehlers T. A., Rusmore M. E. and Farley K. A. (2005) Rapid glacial erosion at 1.8 Ma revealed by $^{4}He/^{3}He$ thermochronometry. *Science* **310**(5754), 1668–1670.

Shuster D. L. and Farley K. A. (2004) $^{4}He/^{3}He$ thermochronometry. *Earth Planet. Sci. Lett.* **217**(1–2), 1–17.

Shuster D. L., Farley K. A., Sisterson J. M. and Burnett D. S. (2004) Quantifying the diffusion kinetics and spatial distributions of radiogenic ^{4}He in minerals containing proton-induced ^{3}He. *Earth Planet. Sci. Lett.* **217**(1–2), 19–32.

Shuster D. L., Flowers R. M. and Farley K. A. (2006) The influence of natural radiation damage on helium diffusion kinetics in apatite. *Earth Planet. Sci. Lett.* **249**(3–4), 148–161.

Summers G. P., Burke E. A., Shapiro P., Messenger S. R. and Walters R. J. (1993) Damage correlations in semiconductors exposed to gamma-radiation, electron-radiation and proton-radiation. *IEEE Trans. Nucl. Sci.* **40**(6), 1372–1379.

Trachenko K., Dove M. T. and Salje E. K. H. (2002) Structural changes in zircon under alpha-decay irradiation. *Phys. Rev. B* **65**(18), 180102.

Weber W. J., Ewing R. C., Catlow C. R. A., de la Rubia T. D., Hobbs L. W., Kinoshita C., Matzke H., Motta A. T., Nastasi M., Salje E. K. H., Vance E. R. and Zinkle S. J. (1998) Radiation effects in crystalline ceramics for the immobilization of high-level nuclear waste and plutonium. *J. Mater. Res.* **13**(6), 1434–1484.

Weber W. J., Ewing R. C. and Meldrum A. (1997) The kinetics of alpha-decay-induced amorphization in zircon and apatite containing weapons-grade plutonium or other actinides. *J. Nucl. Mater.* **250**(2–3), 147–155.

Wolf R. A., Farley K. A. and Silver L. T. (1996) Helium diffusion and low-temperature thermochronometry of apatite. *Geochim. Cosmochim. Acta* **60**(21), 4231–4240.

Young E. J., Myers A. T., Munson E. L. and Conklin N. M. (1969) Mineralogy and geochemistry of fluorapatite from Cerro de Mercado, Durango, Mexico. *United States Geological Survey, Professional Paper* **650-D**, D84–D93.

Zeitler P. K., Herczig A. L., McDougall I. and Honda M. (1987) U–Th–He dating of apatite: a potential thermochronometer. *Geochim. Cosmochim. Acta* **51**, 2865–2868.

Associate editor: Rainer Wieler

Electronic Annex
For Shuster and Farley (2008)

This annex includes 2 tables (Table EA1 and EA2) and 5 figures.

Figure captions:

Figure EA1. ^{3}He-based Arrhenius plots for neutron irradiation experiments for (a) WSAp, (b) Durango Apatite, (c) 01mr59, (d) DYJS5, (e) CJ50 and (f) 00mr18. The control cases (no neutrons) are shown as white squares, 1 hour irradiations as green circles and 90 or 100 hour irradiations as red triangles. All measurements are shown, including points that were not included in the regressions.

Figure EA2: ^{4}He-based Arrhenius plots for the DUR-B samples subjected to (a) 1 hour of annealing at low temperatures, (b) 1 hour of annealing and high temperatures, (c) 10 hours of annealing, (d) 100 and 350 hours of annealing, and (e) 1 hour of annealing using coarse chips experiments. In (e), the D/a^2 values were normalized to a grain size identical to that in DUR-B (see main text). In all panels, only the points used in the regression to obtain Arrhenius parameters are plotted.

Figure EA3. (a) The neutron energy spectrum for the CLILCIT facility at the OSU reactor (REESE, 2007) plotted as the $\log_{10}$(flux) vs. neutron energy (green curve). Nuclear reaction cross sections for the three dominant ^{4}He producing (n,a) reactions on ^{40}Ca, ^{16}O, and ^{19}F are plotted as red, yellow and blue points, respectively. Published reaction cross sections were obtained from the Cross Section Information Storage and Retrieval System (CSISRS) database at the National Nuclear Data Center (http://www.nndc.bnl.gov/). To estimate ^{4}He production rates, the cross sections were parameterized by the solid red, yellow and blue curves shown in (a) and (b).

Figure EA4. The estimated ^{4}He production rate as a function of neutron energy calculated from the parameterized cross sections shown in Fig. EA3 (black curve) plotted against the log of the neutron energy (a) and the neutron energy (b). Also shown for reference in green is the neutron energy spectrum. The red lines note the energy threshold above which ~85 % of the ^{4}He is produced in the reactor.

Figure EA5. ^{4}He/^{3}He thermochronometry applied to the 90 hour neutron irradiation. Shown for two aliquots of 01mr59 are measured isotope ratios for each release step, R_{step} (R=^{4}He/^{3}He), normalized to the bulk ratio R_{bulk}, plotted versus the cumulative ^{3}He release fraction, $\Sigma F^{3}He$ (SHUSTER and FARLEY, 2004). Error bars (1σ) are specified by vertical line through each point. Using the ^{4}He production rate estimated from Figs. EA3 and EA4 and the known ^{3}He diffusion kinetics for this sample, we show four ^{4}He in-growth and diffusion models which correspond to 90 hours at a temperature specified in the figure. The best fitting model is shown in blue, indicating that the samples reached a mean temperature of 260 ^{o}C while in the reactor. Also listed are the predicted and observed ^{4}He concentrations.

References for Electronic Annex:

Reese S. (2007) Personal communication.
Shuster D. L. and Farley K. A. (2004) $^{4}He/^{3}He$ thermochronometry. *Earth and Planetary Science Letters* **217**(1-2), 1-17.

Table EA1a: WSAp_A

Step	T (^{o}C)	t (hr)	[^{3}He] (Matom)	(+/-) 1σ
1	150	0.50	0.08	0.06
2	150	1.25	0.04	0.05
3	150	3.00	0.02	0.04
4	175	1.00	0.04	0.05
5	175	2.00	0.03	0.05
6	200	1.00	0.02	0.05
7	200	1.50	0.04	0.05
8	225	1.00	0.05	0.06
9	225	1.25	0.06	0.05
10	250	0.75	0.14	0.07
11	250	1.25	0.16	0.08
12	240	2.00	0.12	0.06
13	230	3.00	0.08	0.06
14	220	5.00	0.04	0.06
15	235	4.00	0.13	0.07
16	250	2.00	0.13	0.08
17	250	2.50	0.16	0.09
18	265	1.00	0.09	0.06
19	265	1.50	0.12	0.09
20	285	0.50	0.14	0.07
21	285	1.25	0.29	0.11
22	285	1.25	0.26	0.10
23	300	0.50	0.20	0.09
24	300	0.75	0.27	0.09
25	300	1.00	0.30	0.10
26	275	2.00	0.15	0.08
27	275	2.00	0.15	0.08
28	300	1.00	0.22	0.11
29	300	1.25	0.34	0.11
30	325	0.50	0.33	0.10
31	325	0.50	0.37	0.11
32	325	0.50	0.29	0.11
33	340	0.50	0.54	0.14
34	340	0.50	0.50	0.11
35	340	0.75	0.63	0.13
36	365	0.50	1.06	0.18
37	365	0.50	0.96	0.15
38	400	0.50	2.61	0.30
39	425	0.50	5.09	0.36
40	420	0.50	3.20	0.34
41	480	2.00	31.27	1.04
42	500	0.50	7.41	0.53
43	500	0.50	6.52	0.44
44	500	1.00	10.75	0.60
45	500	2.00	17.24	0.78
46	500	3.00	19.09	0.81
47	700	0.20	88.83	1.61
48	800	0.20	138.91	11.55
49	800	0.20	38.16	0.33
50	750	0.40	13.82	0.74
51	700	1.00	5.96	0.43
52	650	1.00	1.29	0.18
53	725	0.50	1.26	0.21
54	725	0.70	0.89	0.18
55	850	0.20	0.61	0.14
56	950	0.10	0.16	0.08
57	950	0.10	0.04	0.05

$(^{4}He^{*}/^{3}He)_{bulk}$ = 9.96

Matom = 10^{6} atoms

Table EA1b: WSAp_B

Step	T (^{o}C)	t (hr)	[^{3}He] (Matom)	(+/-) 1σ
1	250	0.50	0.25	0.09
2	250	1.00	0.19	0.06
3	265	1.00	0.20	0.08
4	265	1.50	0.15	0.07
5	285	0.50	0.13	0.06
6	285	1.25	0.21	0.09
7	285	1.25	0.22	0.08
8	300	0.50	0.11	0.06
9	300	0.75	0.17	0.07
10	300	1.00	0.24	0.09
11	275	2.00	0.08	0.04
12	275	2.00	0.08	0.05
13	300	1.00	0.15	0.06
14	300	1.25	0.18	0.07
15	325	1.00	0.45	0.12
16	325	2.00	0.67	0.13
17	325	3.00	0.74	0.15
18	340	1.00	0.34	0.10
19	340	2.00	0.73	0.16
20	340	3.00	0.87	0.15
21	365	1.00	0.78	0.15
22	365	2.00	1.35	0.22
23	400	1.00	2.05	0.23
24	425	1.00	3.53	0.31
25	420	1.00	2.16	0.27
26	480	1.00	10.18	0.56
27	500	1.00	10.75	0.54
28	500	2.00	13.91	0.66
29	500	3.00	14.64	0.67
30	450	4.00	3.42	0.35
31	400	5.00	0.77	0.17
32	600	0.50	23.66	0.91
33	700	0.20	41.93	1.11
34	800	0.20	71.02	1.44
35	800	0.20	19.33	0.81
36	750	0.40	6.82	0.50
37	700	1.00	3.56	0.29
38	650	1.00	0.79	0.15
39	725	0.50	1.37	0.21
40	775	0.70	2.36	0.23
41	850	0.20	0.60	0.16
42	950	0.20	0.22	0.09

$(^{4}He^{*}/^{3}He)_{bulk}$ = 21.91

Matom = 10^{6} atoms

Table EA1c: WSAp_C

Step	T (^{o}C)	t (hr)	[^{3}He] (Matom)	(+/-) 1σ
1	250	0.50	0.32	0.09
2	250	1.00	0.15	0.06
3	265	1.00	0.24	0.08
4	265	1.50	0.19	0.07
5	285	0.50	0.20	0.07
6	285	1.25	0.22	0.09
7	285	1.25	0.24	0.09
8	300	0.50	0.19	0.08
9	300	0.75	0.22	0.07
10	300	1.00	0.27	0.08
11	275	2.00	0.11	0.06
12	275	2.00	0.10	0.05
13	300	1.00	0.19	0.08
14	300	2.00	0.32	0.11
15	325	1.00	0.61	0.13
16	325	2.00	0.92	0.17
17	325	3.00	1.07	0.19
18	340	1.00	0.65	0.13
19	340	2.00	1.27	0.20
20	340	3.00	1.67	0.22
21	365	1.00	1.45	0.19
22	365	2.00	2.46	0.31
23	400	1.00	4.06	0.36
24	425	1.00	7.78	0.48
25	420	1.00	4.80	0.38
26	480	1.00	22.29	0.78
27	500	1.00	23.46	0.86
28	500	2.00	30.55	1.01
29	500	3.00	31.58	1.01
30	450	4.00	7.91	0.46
31	400	5.00	1.66	0.24
32	600	0.50	60.40	1.57
33	700	0.20	103.06	2.18
34	800	0.20	188.76	3.12
35	800	0.20	60.43	1.26
36	750	0.40	24.67	0.86
37	700	1.00	12.77	0.67
38	650	1.00	2.96	0.28
39	725	0.50	4.62	0.37
40	775	0.70	5.53	0.42
41	850	0.20	0.94	0.16
42	950	0.20	0.21	0.07
43	1050	0.20	0.02	0.02

$(^{4}He^{*}/^{3}He)_{bulk}$ = 592.3

Matom = 10^{6} atoms

Table EA1d: WSAp_D

Step	T (^{o}C)	t (hr)	[^{3}He] (Matom)	(+/-) 1σ
1	200	0.50	0.25	0.16
2	200	0.50	0.04	0.03
3	200	1.00	0.04	0.03
4	200	1.50	0.04	0.04
5	200	2.00	0.02	0.02
6	210	2.00	0.02	0.01
7	220	2.00	0.09	0.04
8	230	2.00	0.11	0.05
9	240	1.50	0.11	0.12
10	250	1.50	0.17	0.06
11	260	1.50	0.21	0.08
12	270	1.00	0.17	0.06
13	280	1.00	0.24	0.09
14	290	0.50	0.15	0.15
15	300	0.50	0.22	0.06
16	310	0.50	0.32	0.08
17	320	0.50	0.43	0.11
18	330	0.50	0.86	0.24
19	340	0.50	0.83	0.26
20	360	0.50	1.44	1.17
21	370	0.50	1.62	2.08
22	380	0.50	1.87	2.17
23	390	0.50	1.89	1.37
24	400	0.50	2.07	1.82
25	410	0.50	2.42	3.99
26	420	0.50	2.97	2.46
27	450	0.50	5.03	0.59
28	500	0.50	11.01	10.72
29	550	0.50	30.09	2.95
30	600	0.50	51.31	5.33
31	650	0.50	73.84	7.00
32	700	0.50	88.92	8.77
33	750	0.50	54.35	5.15
34	700	0.50	88.92	8.77
35	750	0.50	54.35	6.05
36	750	0.50	9.83	1.29
37	800	0.50	2.87	1.43
LS	1100	0.25	0.10	0.10

$(^{4}He^{*}/^{3}He)_{bulk}$ = 97.26

Matom = 10^{6} atoms

Table EA1e: DAp_A

Step	T (^{o}C)	t (hr)	[^{3}He] (Matom)	(+/-) 1σ
1	200	0.50	1.44	0.20
2	200	0.50	0.42	0.11
3	200	1.00	0.65	0.14
4	200	1.50	0.79	0.14
5	190	1.50	0.27	0.08
6	180	2.00	0.15	0.06
7	170	2.50	0.10	0.04
8	160	3.00	0.07	0.04
9	170	3.00	0.13	0.05
10	180	3.00	0.21	0.07
11	190	3.00	0.58	0.13
12	200	2.00	0.54	0.12
13	210	2.00	0.99	0.15
14	220	2.00	1.46	0.22
15	230	2.00	2.45	0.25
16	240	1.50	2.72	0.28
17	250	1.50	3.98	0.32
18	260	1.00	4.02	0.33
19	270	1.00	5.97	0.66
20	280	1.00	11.90	1.47
21	290	0.50	5.73	0.38
22	300	0.50	8.57	0.50
23	310	0.50	10.30	0.69
24	320	0.50	16.19	1.21
25	330	0.50	20.21	0.76
26	340	0.50	25.93	0.72
27	360	0.50	38.56	1.12
28	370	0.50	39.18	0.03
29	380	0.50	37.91	0.03
30	390	0.50	38.32	0.03
31	400	0.50	34.78	0.04
32	410	0.50	31.55	0.03
33	420	0.50	27.96	0.04
34	450	0.50	33.93	1.05
35	500	0.50	32.23	1.17
36	550	0.50	11.87	0.44
37	600	0.50	5.12	0.46
38	650	0.50	4.92	0.37
39	700	0.50	4.38	0.41
40	750	0.50	2.14	0.22
41	800	0.50	0.57	0.11
42	850	0.50	0.20	0.08

$(^{4}He^{*}/^{3}He)_{bulk}$ = 2788

Matom = 10^{6} atoms

Table EA1f: DAp_B

Step	T (^{o}C)	t (hr)	[^{3}He] (Matom)	(+/-) 1σ
1	200	0.50	5.14	0.41
2	200	0.50	1.47	0.20
3	200	0.50	1.24	0.18
4	200	1.00	1.97	0.24
5	200	1.50	2.40	0.28
6	190	1.50	0.98	0.16
7	180	2.00	0.52	0.12
8	170	2.50	0.38	0.09
9	160	3.00	0.18	0.06
10	170	3.00	0.28	0.09
11	180	3.00	0.73	0.13
12	190	3.00	1.37	0.21
13	200	2.00	1.84	0.23
14	210	2.00	3.26	0.34
15	220	2.00	5.55	0.39
16	230	2.00	8.59	0.56
17	250	1.50	15.52	0.79
18	260	1.50	21.07	0.86
19	270	1.00	18.40	0.93
20	280	1.00	26.61	0.91
21	290	0.50	18.21	0.77
22	300	0.50	25.98	0.92
23	310	0.50	35.55	0.99
24	320	0.50	44.95	1.29
25	330	0.50	57.23	2.22
26	340	0.50	69.41	1.63
27	360	0.50	108.95	1.94
28	370	0.50	110.07	1.83
29	380	0.50	106.56	2.47
30	390	0.50	106.35	2.84
31	400	0.50	103.49	1.96
32	410	0.50	100.35	1.69
33	420	0.50	91.30	1.55
34	450	0.50	121.70	2.00
35	500	0.50	149.25	1.98
36	n.d.	n.d.	82.11	5.82
37	600	0.50	25.49	1.50
38	800	0.50	20.90	0.95
39	900	0.50	8.74	0.62
40	1000	0.50	4.18	0.32
41	1200	0.30	0.57	0.14

$(^{4}He^{*}/^{3}He)_{bulk}$ = 3352

Matom = 10^{6} atoms

Table EA1g: DAp_C

Step	T (^{o}C)	t (hr)	[^{3}He] (Matom)	(+/-) 1σ
1	200	0.50	3.34	0.35
2	200	0.50	1.08	0.17
3	200	1.00	1.56	0.23
4	200	1.50	1.67	0.23
5	190	1.50	0.69	0.14
6	180	2.00	0.35	0.11
7	170	2.50	0.20	0.07
8	160	3.00	0.12	0.04
9	170	3.00	0.23	0.07
10	180	3.00	0.59	0.13
11	190	3.00	1.12	0.17
12	200	2.00	1.56	0.21
13	210	2.00	2.95	0.30
14	220	2.00	5.28	0.46
15	230	2.00	9.37	0.52
16	240	1.50	11.27	0.57
17	250	1.50	18.36	0.78
18	260	1.50	26.32	0.93
19	270	1.00	25.06	0.84
20	280	1.00	33.89	1.05
21	290	0.50	22.27	0.77
22	300	0.50	29.46	0.99
23	310	0.50	32.70	1.00
24	320	0.50	33.22	0.99
25	330	0.50	33.62	1.04
26	340	0.50	33.24	1.07
27	360	0.50	49.18	1.20
28	370	0.50	47.93	1.37
29	380	0.50	51.89	1.24
30	390	0.50	52.23	1.40
31	400	0.50	56.96	1.26
32	410	0.50	59.55	1.19
33	420	0.50	61.83	1.47
34	450	0.50	104.03	1.97
35	500	0.50	188.85	2.56
36	550	0.50	167.04	2.26
37	600	0.50	34.65	1.19
38	650	0.50	9.79	0.54
39	700	0.50	5.89	0.45
40	750	0.50	4.11	0.36
41	800	0.50	3.10	0.33
42	850	0.50	1.73	0.23
43	900	0.50	0.76	0.15

(^{4}He*/^{3}He)$_{bulk}$ = 3974

Matom = 10^{6} atoms

Table EA1h: DAp_D

Step	T (^{o}C)	t (hr)	[^{3}He] (Matom)	(+/-) 1σ
1	200	0.50	4.36	0.41
2	200	0.50	1.43	0.18
3	200	0.50	1.18	0.19
4	200	1.00	1.67	0.24
5	200	1.00	1.57	0.22
6	190	1.50	1.12	0.19
7	180	2.00	0.57	0.14
8	170	2.50	0.26	0.08
9	160	3.00	0.15	0.07
10	170	3.00	0.32	0.09
11	180	3.00	0.79	0.16
12	190	3.00	1.79	0.22
13	200	2.00	2.30	0.27
14	210	2.00	4.47	0.34
15	220	2.00	7.62	0.50
16	230	2.00	12.72	0.80
17	240	1.50	15.94	0.73
18	250	1.50	25.16	0.97
19	260	1.50	39.24	1.12
20	270	1.00	36.93	1.08
21	280	1.00	47.33	1.28
22	290	0.50	31.63	0.96
23	300	0.50	39.78	1.07
24	310	0.50	45.81	1.14
25	320	0.50	45.86	1.44
26	330	0.50	45.20	1.65
27	340	0.50	46.30	1.30
28	360	0.50	69.74	1.46
29	370	0.50	62.86	1.62
30	380	0.50	70.33	3.08
31	390	0.50	70.83	1.38
32	400	0.50	73.24	1.83
33	410	0.50	78.92	1.70
34	420	0.50	83.85	1.46
35	450	0.50	178.47	7.45
36	500	0.50	245.97	2.89
37	550	0.50	128.03	1.94
38	600	0.50	34.36	1.14
39	650	0.50	15.00	0.65
40	700	0.50	12.22	0.55
41	800	0.50	12.18	0.65
42	1100	0.50	8.48	0.51

$(^{4}He^{*}/^{3}He)_{bulk}$ = 3954

Matom = 10^{6} atoms

Table EA1i: 01mr59_A

Step	T (^{o}C)	t (hr)	[^{3}He] (Matom)	(+/-) 1σ
1	200	0.50	9.59	0.57
2	200	0.50	3.29	0.34
3	200	0.50	2.64	0.30
4	200	1.00	4.57	0.35
5	200	1.50	5.19	0.41
6	190	1.50	2.47	0.28
7	180	2.00	1.63	0.26
8	170	2.50	0.91	0.16
9	160	3.00	0.46	0.12
10	170	3.00	0.96	0.16
11	180	3.00	1.83	0.25
12	190	3.00	3.64	0.34
13	200	2.00	4.47	0.36
14	210	2.00	7.38	0.43
15	220	2.00	11.88	0.62
16	230	2.00	17.39	0.75
17	250	1.50	27.93	0.92
18	260	1.50	31.66	0.94
19	270	1.00	25.17	0.97
20	280	1.00	28.91	0.99
21	290	0.50	17.37	0.83
22	300	0.50	22.40	0.83
23	310	0.50	26.17	0.94
24	320	0.50	28.77	0.91
25	330	0.50	30.36	0.97
26	340	0.50	32.28	0.95
27	360	0.50	45.71	1.14
28	370	0.50	39.85	1.13
29	380	0.50	38.73	1.14
30	390	0.50	37.99	0.94
31	400	0.50	35.85	0.99
32	410	0.50	34.22	1.18
33	420	0.50	32.43	1.09
34	450	0.50	49.10	1.41
35	550	0.50	104.79	1.72
36	650	0.50	70.46	2.02
37	700	0.50	64.58	1.61
38	800	0.50	95.55	1.84
39	800	0.50	27.37	1.09
40	900	0.50	31.20	1.18
41	1000	0.50	7.28	0.55

$(^{4}He^{*}/^{3}He)_{bulk}$ = 408

Matom = 10^{6} atoms

Table EA1j: 01mr59_B

Step	T (^{o}C)	t (hr)	[^{3}He] (Matom)	(+/-) 1σ	R_{step}/R_{bulk}	(+/-) 1σ
1	200	0.50	0.61	0.13	0.07	0.009
2	200	0.50	0.25	0.08	0.12	0.021
3	200	0.50	0.23	0.07	n.d.	n.d.
4	200	1.00	0.19	0.07	0.23	0.025
5	200	1.50	0.26	0.07	0.22	0.021
6	190	1.50	0.10	0.05	0.28	0.052
7	180	2.00	0.08	0.04	0.20	0.060
8	170	2.50	0.04	0.03	0.23	0.117
9	160	3.00	0.04	0.02	0.23	0.119
10	170	3.00	0.05	0.03	0.23	0.097
11	180	3.00	0.13	0.05	0.19	0.037
12	190	3.00	0.19	0.05	0.47	0.036
13	200	2.00	0.19	0.06	0.33	0.026
14	210	2.00	0.35	0.09	0.34	0.017
15	220	2.00	0.60	0.12	0.34	0.011
16	230	2.00	0.93	0.16	0.39	0.009
17	250	1.50	1.59	0.24	0.57	0.005
18	260	1.50	2.37	0.30	0.47	0.005
19	270	1.00	1.74	0.23	0.62	0.007
20	280	1.00	2.20	0.24	0.68	0.006
21	290	0.50	1.44	0.19	0.72	0.009
22	300	0.50	1.91	0.21	0.78	0.004
23	310	0.50	2.58	0.25	0.74	0.003
24	320	0.50	3.09	0.28	0.81	0.006
25	330	0.50	3.57	0.33	0.84	0.005
26	340	0.50	4.11	0.32	0.86	0.004
27	360	0.50	6.24	0.43	0.93	0.005
28	370	0.50	6.86	0.48	0.88	0.007
29	380	0.50	7.02	0.39	0.93	0.005
30	390	0.50	7.79	0.49	1.00	0.007
31	400	0.50	8.58	0.51	0.98	0.008
32	410	0.50	9.32	0.52	0.98	0.008
33	420	0.50	10.23	0.57	0.98	0.007
34	450	0.50	18.67	0.76	0.99	0.000
35	500	0.50	31.91	1.28	1.03	0.007
36	550	0.50	35.88	1.10	1.06	0.000
37	650	0.50	26.64	0.76	1.08	0.010
38	700	0.50	13.74	0.61	1.10	0.009
39	800	0.50	15.12	0.77	1.17	0.007
40	800	0.50	3.51	0.28	1.32	0.012
41	900	0.50	3.30	0.28	1.28	0.009
42	1000	0.50	1.37	0.20	1.34	0.017

(^{4}He*/^{3}He)$_{bulk}$ = 1341

Matom = 10^{6} atoms

Table EA1k: 01mr59_C

Step	T (^{o}C)	t (hr)	[^{3}He] (Matom)	(+/-) 1σ	R_{step}/R_{bulk}	(+/-) 1σ
1	200	0.50	3.05	0.27	0.07	0.01
2	200	0.50	0.82	0.14	0.20	0.01
3	200	0.50	0.65	0.12	0.23	0.01
4	200	1.00	1.01	0.19	0.32	0.01
5	200	1.00	0.91	0.15	0.27	0.01
6	190	1.50	0.59	0.12	0.31	0.01
7	180	2.00	0.34	0.09	0.36	0.02
8	170	2.50	0.20	0.07	0.39	0.04
9	160	3.00	0.11	0.05	0.41	0.06
10	170	3.00	0.21	0.07	0.43	0.03
11	180	3.00	0.44	0.11	0.39	0.02
12	190	3.00	0.88	0.16	0.37	0.01
13	200	2.00	1.08	0.16	0.38	0.01
14	210	2.00	1.71	0.25	0.44	0.01
15	220	2.00	3.21	0.28	0.42	0.01
16	230	2.00	4.80	0.36	0.47	0.01
17	240	1.50	5.33	0.44	0.51	0.01
18	250	1.50	7.80	0.51	0.54	0.01
19	260	1.50	10.74	0.53	0.61	0.01
20	270	1.00	8.91	0.47	0.69	0.01
21	280	1.00	11.64	0.53	0.72	0.01
22	290	0.50	7.37	0.46	0.78	0.01
23	300	0.50	9.54	0.50	0.79	0.01
24	310	0.50	12.08	0.57	0.82	0.01
25	320	0.50	14.48	0.62	0.83	0.01
26	330	0.50	16.10	0.72	0.89	0.01
27	340	0.50	17.58	0.64	0.90	0.01
28	360	0.50	26.39	0.86	0.94	0.01
29	370	0.50	26.23	0.82	0.96	0.01
30	380	0.50	27.86	0.95	0.95	0.01
31	390	0.50	29.11	0.97	0.99	0.01
32	400	0.50	30.38	0.84	1.01	0.01
33	410	0.50	30.99	1.15	1.03	0.01
34	450	0.50	72.15	1.41	1.04	0.01
35	500	0.50	96.70	1.51	1.05	0.01
36	550	0.50	73.84	1.42	1.07	0.01
37	650	0.50	66.52	1.39	1.10	0.01
38	700	0.50	47.78	1.23	1.10	0.01
39	800	0.50	71.74	1.93	1.18	0.01
40	800	0.50	23.97	0.72	1.16	0.02
41	900	0.50	25.34	0.00	1.02	0.01
42	1200	0.25	13.39	0.00	1.23	0.01

(^{4}He*/^{3}He)$_{bulk}$ = 1347

Matom = 10^{6} atoms

Table EA1l: DYJS5_A

Step	T (^{o}C)	t (hr)	[^{3}He] (Matom)	(+/-) 1σ
1	200	0.50	2.69	0.28
2	200	0.50	0.43	0.11
3	200	0.50	0.27	0.10
4	200	1.00	0.40	0.11
5	200	1.00	0.39	0.10
6	190	1.50	0.22	0.08
7	180	2.00	0.12	0.05
8	170	2.50	0.03	0.01
9	160	3.00	0.03	0.02
10	170	3.00	0.07	0.03
11	180	3.00	0.10	0.05
12	180	3.00	0.15	0.06
13	190	3.00	0.36	0.10
14	200	2.00	0.37	0.10
15	210	2.00	0.69	0.13
16	220	2.00	1.15	0.19
17	230	2.00	1.58	0.25
18	240	1.50	1.83	0.22
19	250	1.50	2.64	0.30
20	260	1.50	3.64	0.38
21	270	1.00	3.20	0.32
22	280	1.00	4.52	0.42
23	280	1.00	3.66	0.33
24	310	0.50	6.60	0.47
25	310	0.50	5.10	0.39
26	330	0.50	9.89	0.66
27	330	0.50	7.33	0.47
28	360	0.50	18.08	0.87
29	360	0.50	11.68	0.71
30	370	0.50	13.70	0.68
31	380	0.50	16.10	0.74
32	390	0.50	17.60	0.81
33	400	0.50	18.67	0.86
34	410	0.50	21.48	0.86
35	430	0.50	38.85	1.14
36	450	0.50	44.11	1.18
37	500	0.50	80.29	1.79
38	550	0.50	59.63	1.31
39	800	0.50	41.77	1.10
40	1100	0.50	0.95	0.18

$(^{4}He^{*}/^{3}He)_{bulk}$ = 1183

Matom = 10^{6} atoms

Table EA1m: CJ50_A

Step	T (^{o}C)	t (hr)	[^{3}He] (Matom)	(+/-) 1σ
1	200	0.5	0.13	0.05
2	200	1.0	0.04	0.02
3	200	1.5	0.05	0.03
4	190	1.5	0.01	0.01
5	180	2.0	0.01	0.01
6	170	2.5	0.02	0.01
7	180	3.0	0.01	0.00
8	190	3.0	0.07	0.03
9	200	2.0	0.04	0.02
10	210	2.0	0.02	0.02
11	220	2.0	0.17	0.07
12	230	2.0	0.18	0.07
13	240	1.5	0.19	0.06
14	250	1.5	0.32	0.09
15	260	1.0	0.35	0.08
16	270	1.0	0.41	0.11
17	280	1.0	0.55	0.12
18	290	0.5	0.39	0.11
19	300	0.5	0.54	0.11
20	310	0.5	0.74	0.15
21	320	0.5	0.98	0.17
22	330	0.5	1.11	0.33
23	340	0.5	1.43	0.20
24	360	0.5	2.50	0.25
25	370	0.5	2.69	0.23
26	380	0.5	3.46	0.29
27	390	0.5	3.85	0.33
28	400	0.5	4.28	0.32
29	410	0.5	4.88	0.34
30	420	0.5	5.55	0.40
31	450	0.5	10.77	0.56
32	500	0.5	22.88	3.00
33	550	0.5	17.39	0.68
34	600	0.5	2.30	0.24
35	650	0.5	0.41	0.10
36	700	0.5	0.38	0.10
37	750	0.5	0.34	0.09
38	800	0.5	0.18	0.05
39	850	0.5	0.03	0.02

$(^{4}He^{*}/^{3}He)_{bulk}$ = 654

Matom = 10^{6} atoms

Table EA1n: 00mr18_A

Step	T (^{o}C)	t (hr)	[^{3}He] (Matom)	(+/-) 1σ
1	200	0.50	0.43	0.12
2	200	0.50	0.15	0.06
3	200	1.00	0.25	0.08
4	200	1.50	0.33	0.10
5	190	1.50	0.16	0.06
6	180	2.00	0.10	0.04
7	170	2.50	0.02	0.02
8	160	3.00	0.02	0.01
9	170	3.00	0.07	0.03
10	180	3.00	0.11	0.04
11	190	3.00	0.22	0.07
12	200	2.00	0.33	0.09
13	210	2.00	0.51	0.12
14	220	2.00	1.18	0.16
15	230	2.00	1.88	0.24
16	240	1.50	2.33	0.26
17	250	1.50	3.34	0.31
18	260	1.00	3.24	0.29
19	270	1.00	4.95	0.37
20	280	1.00	5.74	0.41
21	290	0.50	3.47	0.42
22	300	0.50	4.67	0.39
23	310	0.50	5.64	1.36
24	320	0.50	4.42	0.37
25	330	0.50	3.88	0.35
26	340	0.50	2.36	0.33
27	360	0.50	1.92	0.23
28	370	0.50	1.37	0.18
29	380	0.50	1.11	0.17
30	390	0.50	0.95	0.15
31	400	0.50	0.89	0.16
32	410	0.50	0.88	0.15
33	420	0.50	1.23	0.18
34	450	0.50	1.64	0.20
35	500	0.50	2.22	0.23
36	550	0.50	3.33	0.28
37	600	0.50	5.24	0.41
38	650	0.50	8.04	0.51
39	700	0.50	9.65	0.49
41	800	0.50	11.27	0.51
42	850	0.50	10.22	0.54
43	900	0.50	1.64	0.22
44	950	0.50	6.14	0.40
45	1000	0.50	1.55	0.20
46	1100	0.50	0.51	0.12

(^{4}He*/^{3}He)$_{bulk}$ = 605

Matom = 10^{6} atoms

Table EA2a
Summary of Durango Annealing Experiments
DUR-B Std

NO PRE-TREATMENT

Temperature (^{o}C)	Time (hrs)	FHe	ln(D/a2)	
205	1	4.64E-03	-21.37	
215	1	4.26E-03	-20.39	
225	1	4.98E-03	-19.71	
235	1	6.23E-03	-19.09	
245	1	8.05E-03	-18.48	
255	1	1.09E-02	-17.85	
250	1	6.42E-03	-18.15	
240	1	3.06E-03	-18.78	
230	1	1.60E-03	-19.34	
220	1	7.93E-04	-20.02	
210	1	3.77E-04	-20.75	
200	1	1.86E-04	-21.45	
212	1	4.15E-04	-20.64	
232	1	1.68E-03	-19.22	
252	1	5.60E-03	-17.95	
272	1	1.52E-02	-16.77	
292	1	3.48E-02	-15.60	
320	1	8.43E-02	-14.16	

H1-T75

Temperature (^{o}C)	Time (hrs)	FHe	ln(D/a2)	
75	1	2.83E-06	-36.17	
195	1	2.99E-03	-22.25	point ignored - well off trend line
205	1	3.20E-03	-21.06	
215	1	3.98E-03	-20.27	
225	1	4.99E-03	-19.60	
235	1	6.46E-03	-18.97	
245	1	8.50E-03	-18.36	
255	1	1.13E-02	-17.74	
265	1	1.51E-02	-17.10	
275	1	2.02E-02	-16.49	
285	1	2.70E-02	-15.88	
295	1	3.63E-02	-15.25	
305	1	4.67E-02	-14.67	
315	1	5.69E-02	-14.15	
325	1	6.71E-02	-13.66	

H1-T300

Temperature (^{o}C)	Time (hrs)	FHe	ln(D/a2)
300	1	7.25E-02	-15.84
240	1	1.38E-03	-19.07
240	1	1.28E-03	-19.13
240	1	1.23E-03	-19.15
230	1	6.42E-04	-19.79
220	1	3.30E-04	-20.45

210	1	1.67E-04	-21.13
205	1	1.15E-04	-21.49
195	1	5.88E-05	-22.17
215	1	2.25E-04	-20.82
225	1	4.49E-04	-20.13
235	1	8.66E-04	-19.46
245	1	1.59E-03	-18.84
255	1	2.84E-03	-18.23
265	1	4.93E-03	-17.63
275	1	8.05E-03	-17.06
300	1	2.61E-02	-15.70
325	1	6.15E-02	-14.46
350	1	1.06E-01	-13.41
375	1	1.31E-01	-12.65
400	1	1.33E-01	-12.15

H1-T325

Temperature (^{o}C)	Time (hrs)	FHe	ln(D/a2)
325	1	1.14E-01	-14.90
290	1	2.04E-02	-15.80
290	1	1.89E-02	-15.72
290	1	1.74E-02	-15.67
280	1	9.85E-03	-16.14
270	1	5.54E-03	-16.67
260	1	3.09E-03	-17.22
250	1	1.71E-03	-17.80
240	1	9.39E-04	-18.39
230	1	5.06E-04	-19.00
220	1	2.68E-04	-19.64
210	1	1.37E-04	-20.30
205	1	9.81E-05	-20.64
215	1	1.83E-04	-20.02
225	1	3.57E-04	-19.35
235	1	6.67E-04	-18.72
245	1	1.23E-03	-18.10
255	1	2.22E-03	-17.50
265	1	3.92E-03	-16.91
275	1	6.71E-03	-16.34
285	1	1.10E-02	-15.80
294	1	1.71E-02	-15.28
305	1	2.54E-02	-14.77
315	1	3.61E-02	-14.27
324	1	4.80E-02	-13.80
335	1	6.09E-02	-13.34
345	1	7.15E-02	-12.93
365	1	9.82E-02	-12.31
385	1	1.09E-01	-11.83
405	1	1.07E-01	-11.41
425	1	8.98E-02	-11.05

H1-T350

Temperature (^{o}C)	Time (hrs)	FHe	ln(D/a2)

350	1	9.51E-02	-15.28
289	1	1.07E-02	-16.69
290	1	1.11E-02	-16.54
290	1	1.01E-02	-16.54
280	1	5.87E-03	-17.00
270	1	3.56E-03	-17.47
260	1	2.11E-03	-17.97
250	1	1.20E-03	-18.51
239	1	6.39E-04	-19.14
229	1	3.60E-04	-19.71
220	1	2.05E-04	-20.27
209	1	1.05E-04	-20.93
204	1	7.71E-05	-21.24
215	1	1.54E-04	-20.55
225	1	3.11E-04	-19.85
235	1	5.71E-04	-19.24
244	1	9.69E-04	-18.70
254	1	1.60E-03	-18.19
265	1	2.81E-03	-17.61
274	1	4.62E-03	-17.08
285	1	7.76E-03	-16.52
294	1	1.14E-02	-16.07
305	1	1.74E-02	-15.54
315	1	2.48E-02	-15.06
324	1	3.01E-02	-14.71
335	1	3.93E-02	-14.26
344	1	4.48E-02	-13.94
364	1	6.65E-02	-13.31
384	1	7.84E-02	-12.87
403	1	7.53E-02	-12.64
422	1	6.50E-02	-12.54

H1-T354

Temperature (^{o}C)	Time (hrs)	FHe	ln(D/a2)
354	1	1.50E-01	-14.34
260	1	2.79E-03	-17.58
260	1	2.50E-03	-17.66
250	1	1.51E-03	-18.16
239	1	8.37E-04	-18.74
230	1	5.25E-04	-19.20
220	1	2.45E-04	-19.95
210	1	1.24E-04	-20.63
205	1	9.70E-05	-20.88
215	1	1.68E-04	-20.33
225	1	3.14E-04	-19.70
235	1	5.80E-04	-19.09
245	1	1.02E-03	-18.52
255	1	1.68E-03	-18.01
265	1	2.60E-03	-17.55
274	1	4.48E-03	-16.99
284	1	7.39E-03	-16.45

H1-T365

Temperature (°C)	Time (hrs)	FHe	ln(D/a2)
365	1	1.80E-01	-13.96
260	1	1.25E-03	-18.17
260	1	1.14E-03	-18.26
250	1	6.39E-04	-18.83
240	1	3.73E-04	-19.37
230	1	2.09E-04	-19.94
220	1	1.19E-04	-20.51
210	1	6.66E-05	-21.09
205	1	5.03E-05	-21.37
215	1	8.60E-05	-20.83
225	1	1.52E-04	-20.26
235	1	2.73E-04	-19.68
245	1	4.76E-04	-19.12
255	1	8.24E-04	-18.56
265	1	1.41E-03	-18.02
275	1	2.33E-03	-17.50

H1-T375

Temperature (°C)	Time (hrs)	FHe	ln(D/a2)
375	1	1.99E-01	-13.74
240	1	5.53E-04	-18.87
230	1	3.01E-04	-19.48
220	1	1.70E-04	-20.05
210	1	9.36E-05	-20.64
205	1	6.87E-05	-20.95
195	1	3.90E-05	-21.52
215	1	1.18E-04	-20.41
225	1	2.07E-04	-19.85
235	1	3.60E-04	-19.29
245	1	6.23E-04	-18.74
255	1	1.09E-03	-18.18
265	1	1.82E-03	-17.66
275	1	2.98E-03	-17.15

H1-T397

Temperature (°C)	Time (hrs)	FHe	ln(D/a2)
397	1	2.14E-01	-13.59
240	1	4.59E-04	-18.97
230	1	2.61E-04	-19.54
220	1	1.54E-04	-20.06
210	1	9.11E-05	-20.59
205	1	6.90E-05	-20.86
195	1	4.12E-05	-21.38
215	1	1.15E-04	-20.35
225	1	1.89E-04	-19.85
235	1	3.16E-04	-19.34
245	1	5.45E-04	-18.79
254	1	9.32E-04	-18.25
264	1	1.52E-03	-17.75
274	1	2.40E-03	-17.29

H1-T414

Temperature (°C)	Time (hrs)	FHe	ln(D/a2)
414	1	3.13E-01	-12.76
239	1	4.61E-04	-18.48
240	1	4.58E-04	-18.49
240	1	4.64E-04	-18.47
230	1	2.54E-04	-19.07
220	1	1.52E-04	-19.59
210	1	9.48E-05	-20.06
205	1	6.82E-05	-20.39
194	1	4.01E-05	-20.92
215	1	1.16E-04	-19.85
224	1	1.88E-04	-19.37
235	1	3.15E-04	-18.85
245	1	5.38E-04	-18.32
254	1	8.57E-04	-17.85
265	1	1.47E-03	-17.30
274	1	2.16E-03	-16.91
299	1	6.10E-03	-15.86
324	1	1.41E-02	-14.98
349	1	2.84E-02	-14.19
375	1	4.83E-02	-13.51
399	1	6.36E-02	-13.02

H1-T450

Temperature (°C)	Time (hrs)	FHe	ln(D/a2)
450	1	8.71E-01	-10.04
240	1	1.33E-04	-17.35
240	1	1.29E-04	-17.37
240	1	1.25E-04	-17.40
230	1	7.89E-05	-17.86
220	1	4.95E-05	-18.33
210	1	3.07E-05	-18.81
205	1	2.38E-05	-19.06
195	1	1.48E-05	-19.54
215	1	3.82E-05	-18.59
225	1	6.00E-05	-18.14
235	1	9.44E-05	-17.68
255	1	2.23E-04	-16.82
265	1	3.31E-04	-16.42
275	1	4.89E-04	-16.03
290	1	8.59E-04	-15.46
305	1	1.46E-03	-14.92
320	1	2.38E-03	-14.42
340	1	4.36E-03	-13.78
360	1	7.27E-03	-13.21
380	1	1.08E-02	-12.75
400	1	1.41E-02	-12.36
420	1	1.56E-02	-12.08
440	1	1.49E-02	-11.91

H1-T500

Temperature (°C)	Time (hrs)	FHe	ln(D/a2)
500	1	9.38E-01	-9.65
240	1	4.58E-05	-17.69
240	1	3.04E-05	-18.10
240	1	2.98E-05	-18.12
230	1	2.06E-05	-18.49
220	1	1.39E-05	-18.88
210	1	9.54E-06	-19.26
205	1	7.57E-06	-19.49
195	1	5.03E-06	-19.90
216	1	1.09E-05	-19.12
225	1	1.58E-05	-18.75
235	1	2.29E-05	-18.38
255	1	4.91E-05	-17.62
265	1	7.11E-05	-17.24
275	1	9.75E-05	-16.93
290	1	1.61E-04	-16.42
304	1	2.54E-04	-15.97
320	1	4.06E-04	-15.49
338	1	6.92E-04	-14.95
360	1	1.20E-03	-14.38
379	1	1.89E-03	-13.90
397	1	2.59E-03	-13.54
416	1	3.42E-03	-13.21
430	1	3.72E-03	-13.06

H10-T250

Temperature (°C)	Time (hrs)	FHe	ln(D/a2)
250	10	5.62E-02	-18.66
240	1	5.78E-02	-19.23
230	1	5.85E-02	-19.94
220	1	5.89E-02	-20.63
210	1	5.91E-02	-21.32
205	1	5.92E-02	-21.68
195	1	5.93E-02	-22.38
215	1	5.95E-02	-21.01
225	1	6.00E-02	-20.32
235	1	6.10E-02	-19.65
245	1	6.28E-02	-18.95
255	1	6.60E-02	-18.36
265	1	7.19E-02	-17.68
275	1	8.16E-02	-17.08
300	1	1.09E-01	-15.79
325	1	1.76E-01	-14.47
350	1	2.94E-01	-13.30
375	1	4.46E-01	-12.44
400	1	5.91E-01	-11.94

H10-T275

Temperature (°C)	Time (hrs)	FHe	ln(D/a2)

275	10	1.14E-01	-17.21
240	1	9.17E-04	-19.00
229	1	4.84E-04	-19.63
219	1	2.48E-04	-20.30
209	1	1.29E-04	-20.95
205	1	9.55E-05	-21.25
195	1	4.92E-05	-21.91
215	1	1.80E-04	-20.62
225	1	3.50E-04	-19.95
234	1	6.87E-04	-19.27
245	1	1.27E-03	-18.64
254	1	2.25E-03	-18.06
265	1	4.00E-03	-17.45
275	1	6.57E-03	-16.91
299	1	2.13E-02	-15.62
325	1	5.37E-02	-14.42
349	1	9.34E-02	-13.45
374	1	1.14E-01	-12.79
399	1	1.14E-01	-12.36

H10-T300

Temperature (^{o}C)	Time (hrs)	FHe	ln(D/a2)
300	10	2.27E-01	-15.77
240	1	6.48E-04	-18.56
239	1	5.82E-04	-18.66
239	1	5.52E-04	-18.71
230	1	3.32E-04	-19.22
220	1	1.82E-04	-19.82
210	1	9.94E-05	-20.42
205	1	7.33E-05	-20.72
194	1	3.60E-05	-21.43
214	1	1.32E-04	-20.13
224	1	2.27E-04	-19.59
234	1	4.14E-04	-18.99
245	1	7.70E-04	-18.37
255	1	1.38E-03	-17.78
265	1	2.46E-03	-17.19
274	1	3.99E-03	-16.69
298	1	1.25E-02	-15.50
324	1	3.41E-02	-14.38
349	1	7.56E-02	-13.34
372	1	1.13E-01	-12.56
398	1	1.33E-01	-11.95

H10-T315

Temperature (^{o}C)	Time (hrs)	FHe	ln(D/a2)
315	10	2.75E-01	-15.35
240	1	4.38E-04	-18.71
240	1	3.86E-04	-18.83
240	1	3.71E-04	-18.87
230	1	2.09E-04	-19.44
220	1	1.14E-04	-20.05

210	1	6.21E-05	-20.65
205	1	4.52E-05	-20.97
195	1	2.53E-05	-21.55
215	1	8.06E-05	-20.39
225	1	1.48E-04	-19.79
235	1	2.70E-04	-19.18
245	1	4.81E-04	-18.60
255	1	8.68E-04	-18.01
265	1	1.53E-03	-17.44
275	1	2.54E-03	-16.92
300	1	8.44E-03	-15.70
325	1	2.39E-02	-14.58
350	1	5.27E-02	-13.63
375	1	8.80E-02	-12.84
400	1	1.10E-01	-12.26

H10-T330

Temperature (^{o}C)	Time (hrs)	FHe	ln(D/a2)
330	10	2.59E-01	-15.48
240	1	3.32E-04	-19.06
239	1	2.89E-04	-19.19
240	1	3.04E-04	-19.14
230	1	1.71E-04	-19.72
219	1	9.11E-05	-20.35
210	1	5.29E-05	-20.89
204	1	3.82E-05	-21.22
195	1	2.31E-05	-21.72
215	1	7.21E-05	-20.58
225	1	1.27E-04	-20.02
235	1	2.19E-04	-19.47
245	1	3.80E-04	-18.92
254	1	6.32E-04	-18.40
264	1	1.07E-03	-17.87
274	1	1.77E-03	-17.37
299	1	5.57E-03	-16.20
324	1	1.56E-02	-15.12
348	1	3.39E-02	-14.23
374	1	6.24E-02	-13.42
399	1	8.76E-02	-12.79

H10-T345

Temperature (^{o}C)	Time (hrs)	FHe	ln(D/a2)
345	10	2.79E-01	-15.32
240	1	2.37E-04	-19.30
240	1	2.24E-04	-19.36
240	1	2.23E-04	-19.36
230	1	1.33E-04	-19.88
220	1	7.85E-05	-20.40
210	1	4.57E-05	-20.94
205	1	3.56E-05	-21.19
195	1	2.06E-05	-21.74
215	1	5.89E-05	-20.69

225	1	9.96E-05	-20.17
235	1	1.68E-04	-19.64
245	1	2.78E-04	-19.14
255	1	4.61E-04	-18.63
265	1	7.43E-04	-18.15
275	1	1.19E-03	-17.67
300	1	3.43E-03	-16.60
325	1	8.78E-03	-15.64
350	1	2.02E-02	-14.74
375	1	4.06E-02	-13.91
400	1	6.73E-02	-13.19

H100-T250

Temperature (^{o}C)	Time (hrs)	FHe	ln(D/a2)
250	100	8.93E-02	-20.02
239	1	7.16E-04	-19.51
239	1	7.23E-04	-19.50
239	1	7.21E-04	-19.49
229	1	3.92E-04	-20.09
219	1	2.03E-04	-20.75
209	1	1.03E-04	-21.42
205	1	7.22E-05	-21.78
195	1	3.68E-05	-22.45
215	1	1.38E-04	-21.13
225	1	2.75E-04	-20.44
235	1	5.20E-04	-19.79
245	1	9.63E-04	-19.17
255	1	1.76E-03	-18.55
265	1	3.13E-03	-17.95
275	1	5.39E-03	-17.36

H100-T275

Temperature (^{o}C)	Time (hrs)	FHe	ln(D/a2)
250	100	3.27E-01	-17.27
249	1	5.01E-04	-18.34
239	1	2.86E-04	-18.90
239	1	2.74E-04	-18.94
239	1	2.75E-04	-18.94
230	1	1.60E-04	-19.48
219	1	8.62E-05	-20.09
209	1	4.60E-05	-20.72
204	1	3.26E-05	-21.07
194	1	1.77E-05	-21.68
214	1	5.76E-05	-20.50
224	1	1.09E-04	-19.86
234	1	2.09E-04	-19.21
244	1	3.86E-04	-18.59
255	1	7.17E-04	-17.97
264	1	1.24E-03	-17.42
274	1	2.14E-03	-16.86
299	1	7.34E-03	-15.61
324	1	2.25E-02	-14.43

349	1	5.47E-02	-13.39
374	1	1.01E-01	-12.49
399	1	1.28E-01	-11.84

H100-T300

Temperature (^{o}C)	Time (hrs)	FHe	ln(D/a2)
300	100	2.88E-01	-17.55
240	1	1.01E-04	-20.11
240	1	9.10E-05	-20.22
240	1	8.95E-05	-20.23
230	1	5.11E-05	-20.79
220	1	2.92E-05	-21.35
210	1	1.66E-05	-21.91
205	1	1.22E-05	-22.22
195	1	7.10E-06	-22.77
215	1	2.11E-05	-21.67
225	1	3.74E-05	-21.10
235	1	6.58E-05	-20.54
245	1	1.14E-04	-19.99
255	1	1.97E-04	-19.44
265	1	3.39E-04	-18.90
275	1	5.63E-04	-18.39
300	1	1.82E-03	-17.21
325	1	5.08E-03	-16.17
350	1	1.24E-02	-15.23
375	1	2.47E-02	-14.47
400	1	3.85E-02	-13.89

H100-T325

Temperature (^{o}C)	Time (hrs)	FHe	ln(D/a2)
325	100	7.70E-01	-15.10
250	1	2.07E-04	-17.53
240	1	1.30E-05	-20.30
240	1	1.22E-05	-20.36
240	1	1.20E-05	-20.38
230	1	7.35E-06	-20.87
220	1	4.09E-06	-21.45
210	1	2.23E-06	-22.06
205	1	1.44E-06	-22.50
195	1	6.65E-07	-23.27
215	1	2.89E-06	-21.80
225	1	4.88E-06	-21.27
235	1	9.18E-06	-20.64
245	1	1.61E-05	-20.08
255	1	2.59E-05	-19.61
265	1	4.02E-05	-19.16
275	1	6.93E-05	-18.62
300	1	1.80E-04	-17.66
325	1	5.05E-04	-16.63
350	1	1.24E-03	-15.73
375	1	2.74E-03	-14.93
400	1	5.31E-03	-14.25

H350-T250

Temperature (^{o}C)	Time (hrs)	FHe	ln(D/a2)
250	350	2.95E-01	-18.75
250	1	4.94E-04	-18.50
240	1	2.85E-04	-19.04
240	1	2.88E-04	-19.03
240	1	2.91E-04	-19.02
230	1	1.56E-04	-19.64
220	1	8.10E-05	-20.30
210	1	4.33E-05	-20.92
205	1	2.97E-05	-21.30
215	1	5.83E-05	-20.63
225	1	1.13E-04	-19.97
235	1	2.06E-04	-19.37
245	1	3.81E-04	-18.75
255	1	7.17E-04	-18.11
265	1	1.27E-03	-17.54
275	1	2.15E-03	-17.00
285	1	3.60E-03	-16.48
295	1	6.11E-03	-15.92
305	1	9.81E-03	-15.42
315	1	1.47E-02	-14.96
325	1	2.21E-02	-14.47

H350-T270

Temperature (^{o}C)	Time (hrs)	FHe	ln(D/a2)
270	350	3.59E-01	-18.31
249	1	2.14E-04	-19.06
239	1	1.21E-04	-19.63
239	1	1.19E-04	-19.64
239	1	1.17E-04	-19.66
230	1	6.94E-05	-20.19
219	1	3.72E-05	-20.81
209	1	2.00E-05	-21.43
204	1	1.39E-05	-21.79
214	1	2.62E-05	-21.16
224	1	4.77E-05	-20.56
235	1	9.18E-05	-19.90
244	1	1.60E-04	-19.35
254	1	2.79E-04	-18.79
264	1	4.80E-04	-18.25
275	1	8.56E-04	-17.67
284	1	1.35E-03	-17.20
294	1	2.13E-03	-16.74
304	1	3.59E-03	-16.21
314	1	5.19E-03	-15.83
324	1	7.58E-03	-15.42

Table EA2b
Summary of Durango Annealing Experiments
DUR-C CHIPS
Number beside aliquot name is equivalent sphere radius
Diffusivities scaled to r=85 um (see text)

BH0-T0 0.0686

Temperature (^{o}C)	Time (hrs)	FHe	ln(D/a2)
205	1	2.86E-04	-22.18
215	1	2.67E-04	-21.18
225	1	3.05E-04	-20.52
235	1	3.94E-04	-19.87
245	1	5.16E-04	-19.24
255	1	6.79E-04	-18.63
250	1	3.98E-04	-18.94
240	1	2.00E-04	-19.52
230	1	9.78E-05	-20.18
265	1	7.72E-04	-17.99
275	1	1.13E-03	-17.37
285	1	1.55E-03	-16.79
295	1	2.15E-03	-16.19
305	1	2.90E-03	-15.60
314	1	3.85E-03	-15.03
324	1	4.97E-03	-14.50
334	1	6.33E-03	-13.98
344	1	7.73E-03	-13.52
354	1	9.09E-03	-13.12
364	1	1.05E-02	-12.71
374	1	1.19E-02	-12.37

BH1-T150 0.0653

Temperature (^{o}C)	Time (hrs)	FHe	ln(D/a2)
150	1	1.67E-05	-27.97
204	1	4.73E-04	-21.21
214	1	4.75E-04	-20.15
225	1	5.65E-04	-19.44
234	1	6.34E-04	-18.93
244	1	9.16E-04	-18.21
254	1	1.19E-03	-17.62
249	1	7.21E-04	-17.88
240	1	3.44E-04	-18.51
229	1	1.88E-04	-19.07
264	1	1.33E-03	-16.98
275	1	2.12E-03	-16.27
284	1	2.37E-03	-15.91
294	1	4.37E-03	-15.01
304	1	5.23E-03	-14.53
314	1	7.41E-03	-13.88
324	1	7.74E-03	-13.57
334	1	9.43E-03	-13.13
344	1	1.94E-02	-12.07
354	1	1.59E-02	-11.98

364	1	1.76E-02	-11.65
374	1	1.92E-02	-11.36
384	1	2.21E-02	-11.03
394	1	2.07E-02	-10.92

BH1-T250 0.0905

Temperature (^{o}C)	Time (hrs)	FHe	ln(D/a2)
250	1	1.20E-03	-18.77
240	1	3.20E-04	-19.27
240	1	2.65E-04	-19.26
240	1	2.32E-04	-19.25
230	1	1.11E-04	-19.90
220	1	5.45E-05	-20.58
210	1	2.65E-05	-21.28
205	1	1.83E-05	-21.64
215	1	3.61E-05	-20.95
225	1	7.08E-05	-20.25
235	1	1.33E-04	-19.58
245	1	2.40E-04	-18.91
255	0.5	2.10E-04	-18.27
265	0.5	3.58E-04	-17.64
275	0.5	5.78E-04	-17.02
285	0.5	8.73E-04	-16.42
295	0.5	1.27E-03	-15.82
305	0.5	1.85E-03	-15.19
315	0.5	2.45E-03	-14.64
325	0.5	3.31E-03	-14.06
345	0.5	6.40E-03	-13.06
370	0.5	1.25E-02	-11.94

BH1-T325 0.0605

Temperature (^{o}C)	Time (hrs)	FHe	ln(D/a2)
325	1	1.04E-02	-15.24
290	1	1.23E-03	-16.62
290	1	1.13E-03	-16.61
290	1	1.04E-03	-16.60
280	1	6.20E-04	-17.06
270	1	3.81E-04	-17.51
250	1	1.09E-04	-18.74
240	1	5.97E-05	-19.34
230	1	3.29E-05	-19.94
220	1	1.69E-05	-20.60
210	1	8.95E-06	-21.24
215	1	1.19E-05	-20.95
225	1	2.27E-05	-20.30
235	1	4.32E-05	-19.66
245	1	7.94E-05	-19.05
255	1	1.45E-04	-18.44
265	1	2.55E-04	-17.86
275	1	4.29E-04	-17.32
274	1	4.29E-04	-17.29
284	1	7.13E-04	-16.75

305	1	1.82E-03	-15.74
325	1	3.98E-03	-14.81
344	1	7.68E-03	-13.90
365	1	1.31E-02	-13.04
384	1	1.79E-02	-12.34
404	1	2.40E-02	-11.69
424	1	2.80E-02	-11.21
444	1	3.39E-02	-10.72

BH1-T350 0.0651

Temperature (^{o}C)	Time (hrs)	FHe	ln(D/a2)
350	1	1.98E-02	-13.81
290	1	8.79E-04	-16.21
290	1	8.47E-04	-16.21
290	1	8.19E-04	-16.20
280	1	4.80E-04	-16.71
270	1	2.79E-04	-17.23
260	1	1.59E-04	-17.79
250	1	8.86E-05	-18.37
240	1	4.91E-05	-18.95
230	1	2.66E-05	-19.57
220	1	1.41E-05	-20.20
210	1	7.18E-06	-20.87
205	1	5.03E-06	-21.23
215	1	9.90E-06	-20.55
225	1	1.91E-05	-19.89
235	1	3.56E-05	-19.27
245	1	6.56E-05	-18.66
255	1	1.18E-04	-18.07
265	1	2.04E-04	-17.51
275	1	3.50E-04	-16.96
285	1	5.79E-04	-16.44
295	1	9.17E-04	-15.95
305	1	1.40E-03	-15.48
315	1	2.07E-03	-15.03
325	1	2.88E-03	-14.61
345	1	5.79E-03	-13.78
365	1	1.01E-02	-13.02
385	1	1.56E-02	-12.28
405	1	2.15E-02	-11.66

BH1-T375 0.0731

Temperature (^{o}C)	Time (hrs)	FHe	ln(D/a2)
375	1	3.19E-02	-12.62
290	1	3.26E-02	-15.77
290	1	3.32E-02	-15.74
290	1	3.39E-02	-15.76
280	1	3.43E-02	-16.22
270	1	3.46E-02	-16.71
260	1	3.47E-02	-17.23
250	1	3.48E-02	-17.81
240	1	3.48E-02	-18.36

230	1	3.49E-02	-18.94
220	1	3.49E-02	-19.55
210	1	3.49E-02	-20.18
205	1	3.49E-02	-20.50
215	1	3.49E-02	-19.89
225	1	3.49E-02	-19.26
235	1	3.50E-02	-18.65
245	1	3.50E-02	-18.06
255	1	3.51E-02	-17.50
265	1	3.53E-02	-16.96
275	1	3.56E-02	-16.44
285	1	3.61E-02	-15.95
295	1	3.69E-02	-15.49
305	1	3.81E-02	-15.06
315	1	3.98E-02	-14.65
325	1	4.22E-02	-14.26
345	1	4.69E-02	-13.51
365	1	5.50E-02	-12.78
385	1	6.78E-02	-12.14
405	1	8.61E-02	-11.54
425	1	1.10E-01	-10.99
445	1	1.41E-01	-10.50

BH1-T391 0.0808

Temperature (^{o}C)	Time (hrs)	FHe	ln(D/a2)
391	1	5.44E-02	-11.33
290	1	6.52E-04	-15.04
290	1	6.65E-04	-15.01
290	1	6.62E-04	-15.00
280	1	4.14E-04	-15.46
270	1	2.57E-04	-15.93
260	1	1.55E-04	-16.43
250	1	9.25E-05	-16.95
240	1	5.58E-05	-17.45
230	1	3.26E-05	-17.99
220	1	1.89E-05	-18.53
210	1	1.10E-05	-19.08
205	1	8.18E-06	-19.37
215	1	1.41E-05	-18.83
225	1	2.40E-05	-18.29
235	1	4.15E-05	-17.75
245	1	6.94E-05	-17.23
255	1	1.18E-04	-16.70
265	1	1.97E-04	-16.18
275	1	3.18E-04	-15.70
285	1	5.09E-04	-15.22
295	1	7.80E-04	-14.78
304	1	1.16E-03	-14.37
313	1	1.62E-03	-14.01
324	1	2.39E-03	-13.59

BH1-T415 0.0702

Temperature (^{o}C)	Time (hrs)	FHe	ln(D/a2)
415	1	5.94E-02	-11.32
290	1	4.46E-04	-15.50
290	1	4.38E-04	-15.51
290	1	4.33E-04	-15.52
280	1	2.74E-04	-15.97
270	1	1.72E-04	-16.43
260	1	1.06E-04	-16.91
250	1	6.40E-05	-17.42
240	1	3.73E-05	-17.96
230	1	2.20E-05	-18.48
220	1	1.29E-05	-19.02
210	1	7.31E-06	-19.58
205	1	5.45E-06	-19.88
215	1	9.26E-06	-19.35
225	1	1.70E-05	-18.74
235	1	2.93E-05	-18.19
245	1	4.99E-05	-17.66
255	1	7.97E-05	-17.19
265	0.5	6.99E-05	-16.63
275	0.5	1.05E-04	-16.22
300	0.5	3.33E-04	-15.06
325	0.5	8.14E-04	-14.16
350	0.5	1.90E-03	-13.29

Shuster and Farley (2008)
Figure EA1a

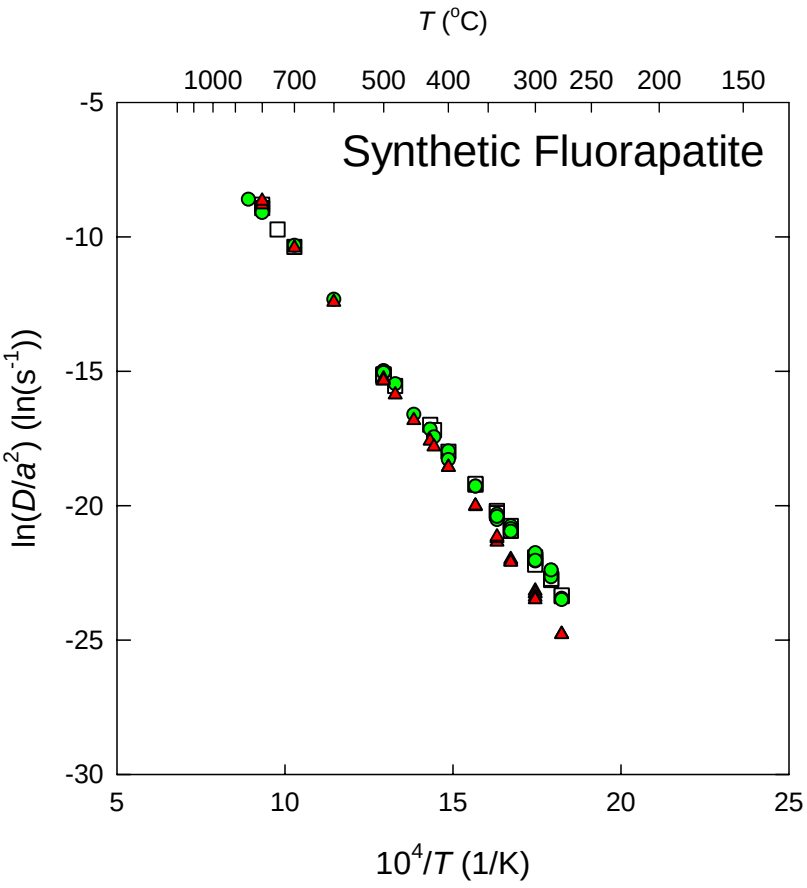

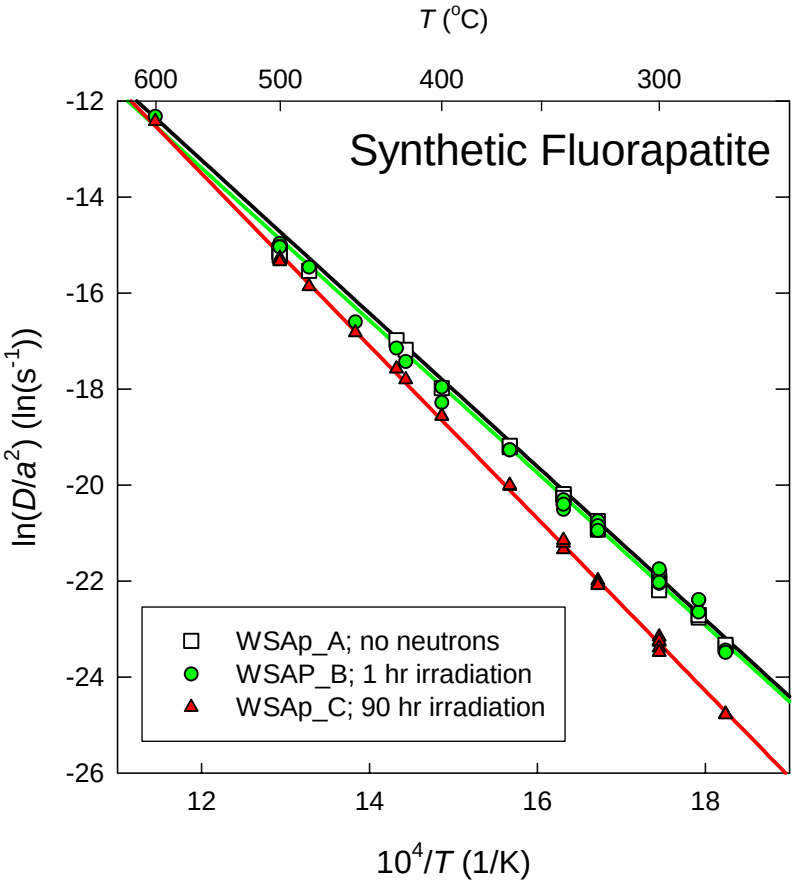

Shuster and Farley (2008)
Figure EA1b

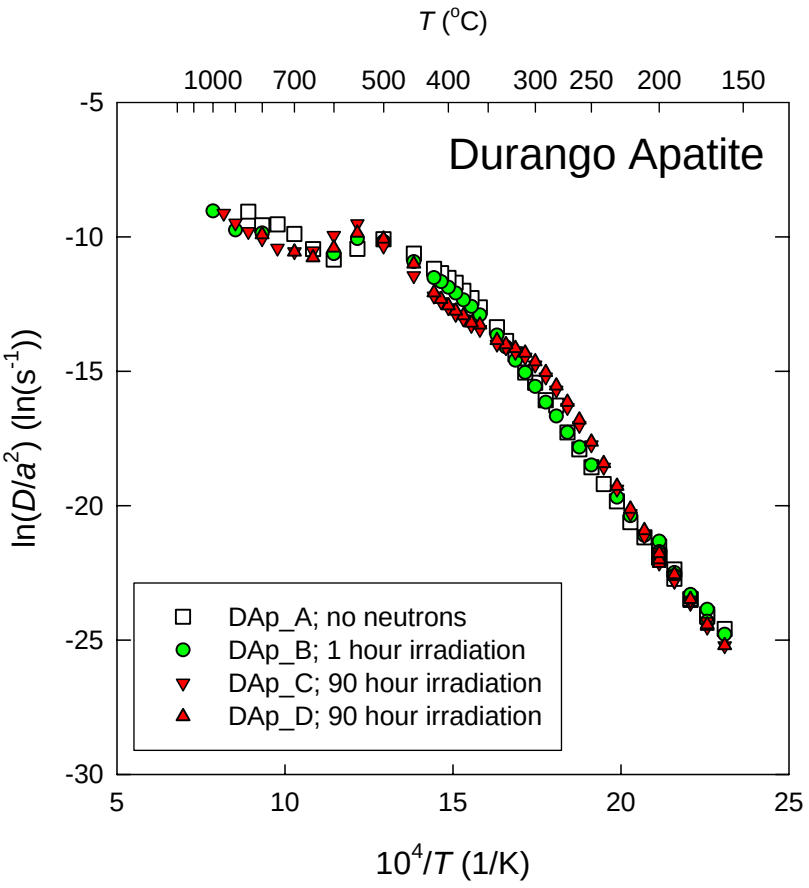

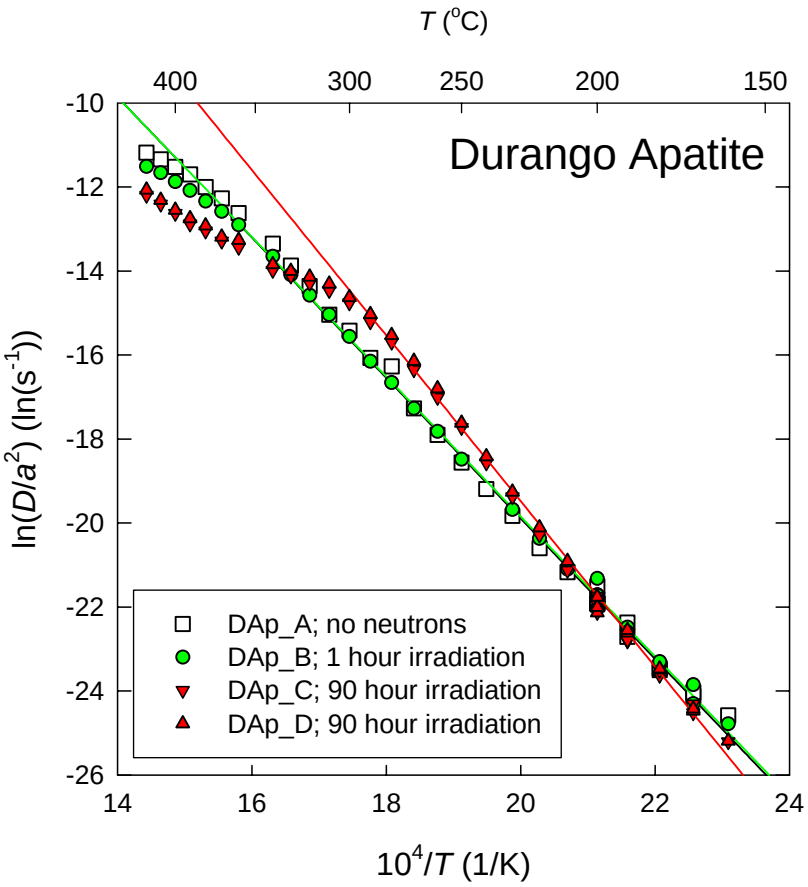

Shuster and Farley (2008)
Figure EA1c

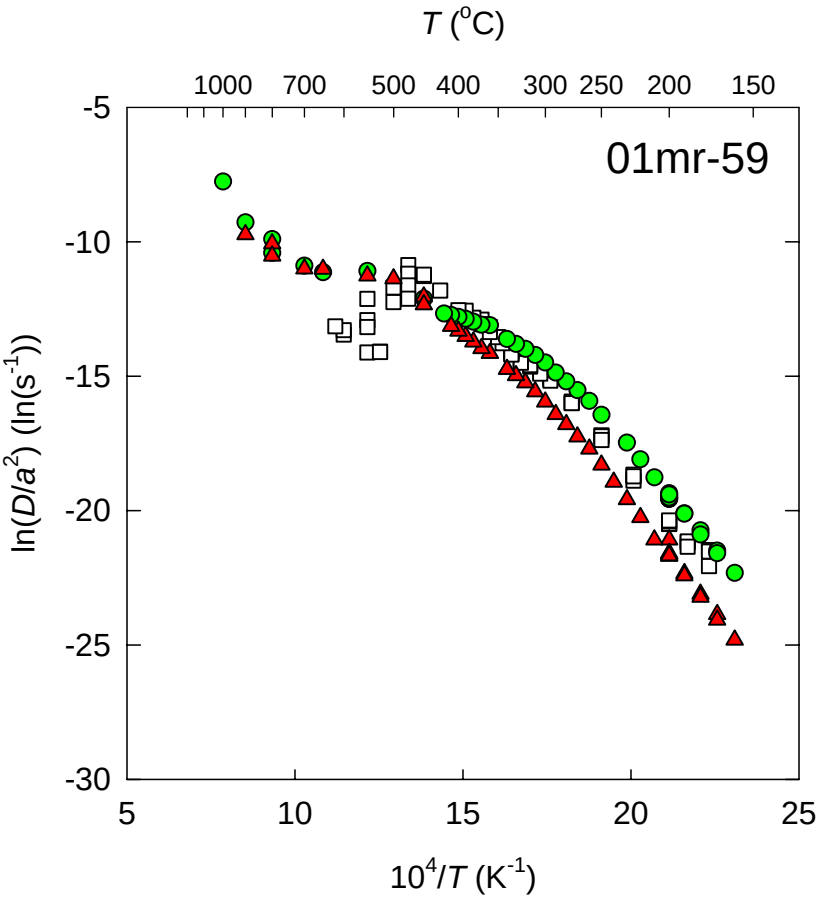

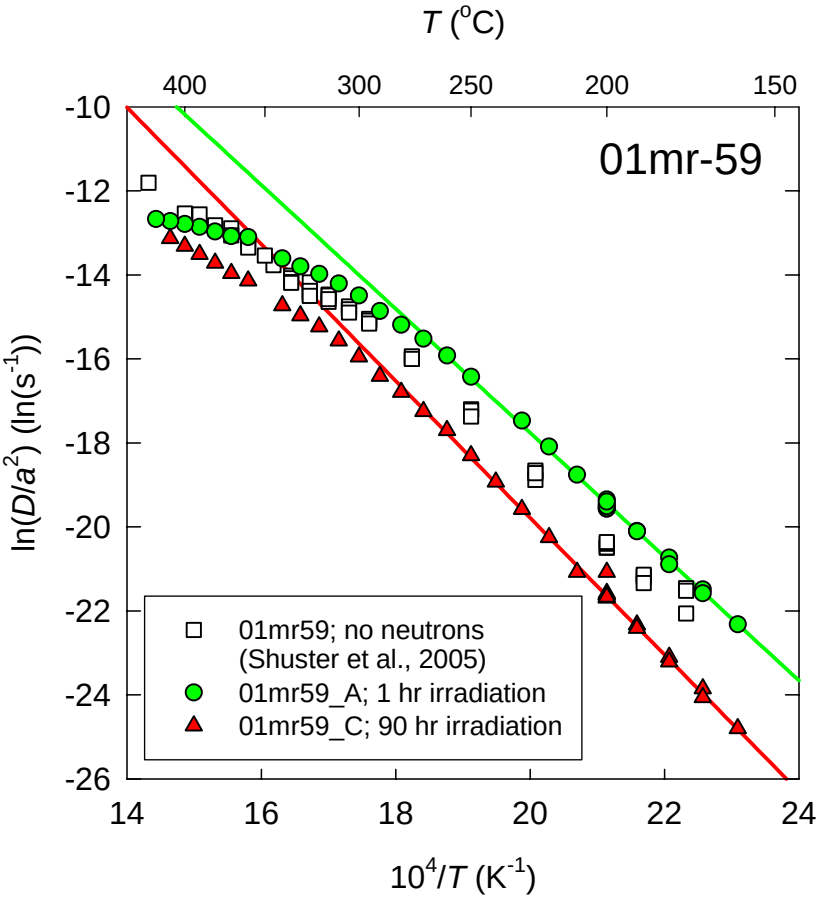

Shuster and Farley (2008)
Figure EA1d

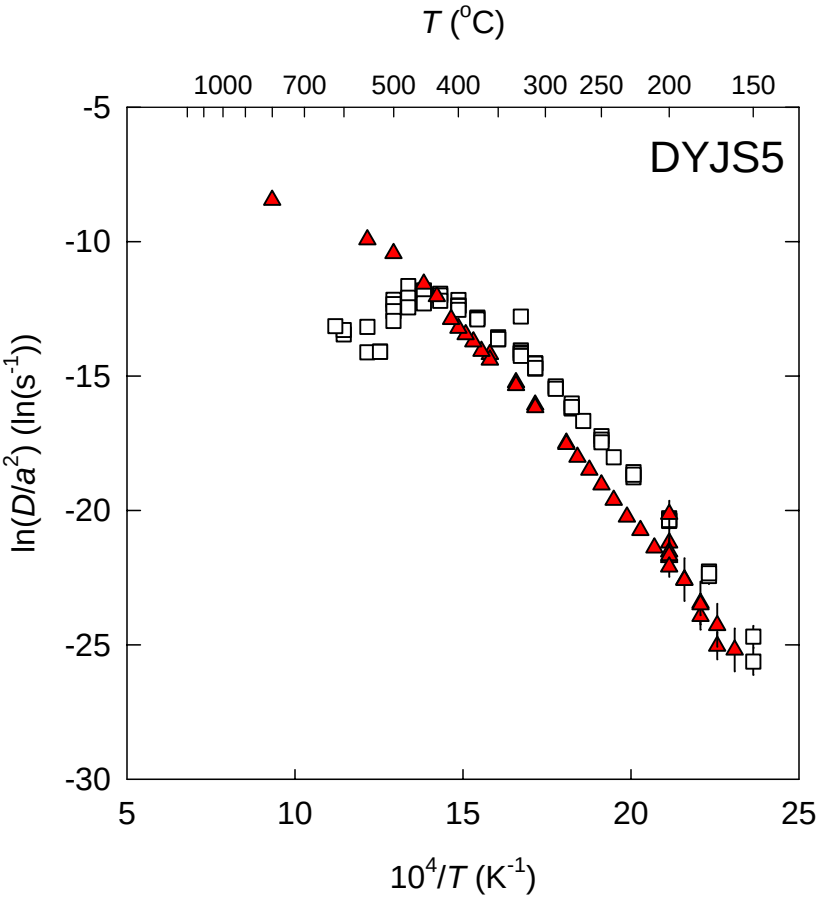

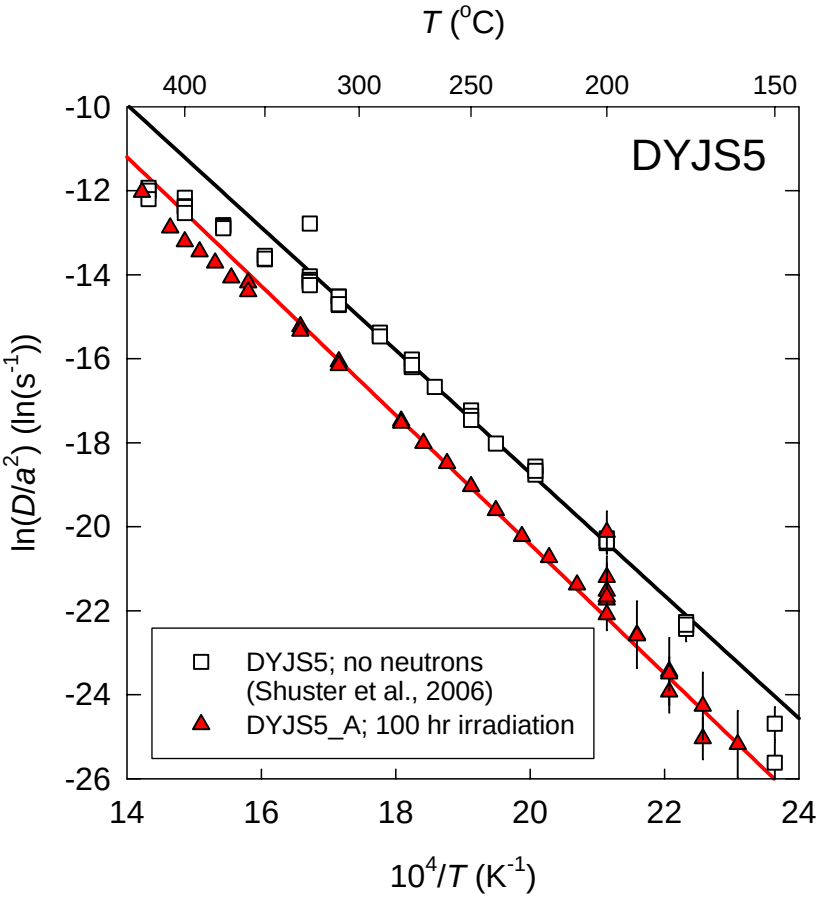

Shuster and Farley (2008)
Figure EA1e

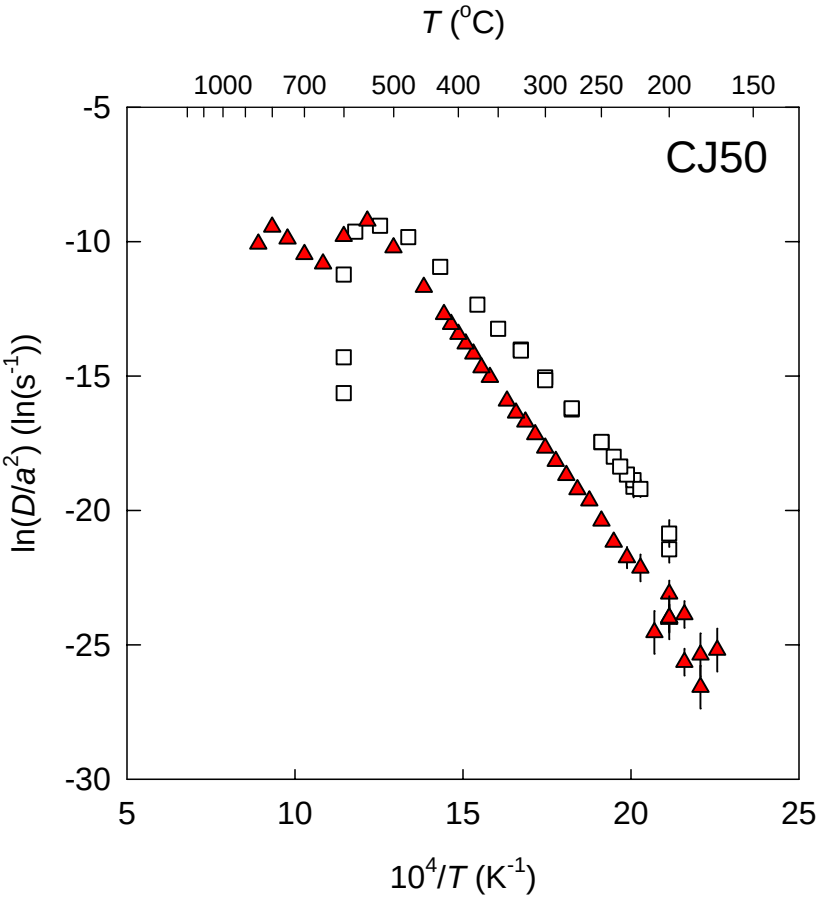

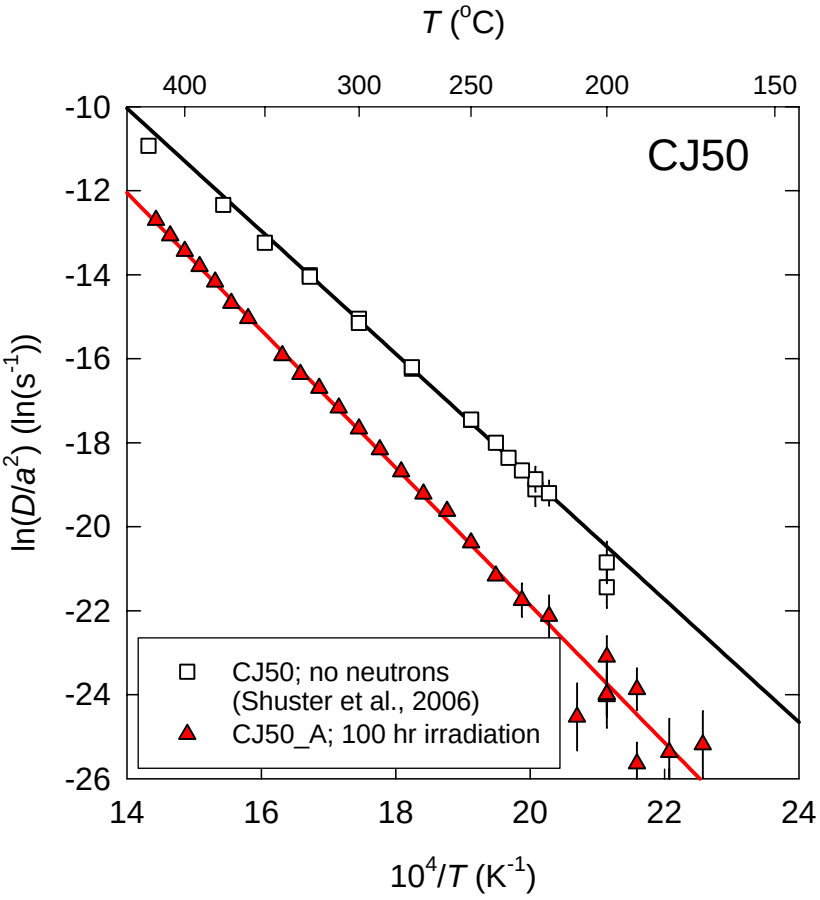

Shuster and Farley (2008)
Figure EA1f

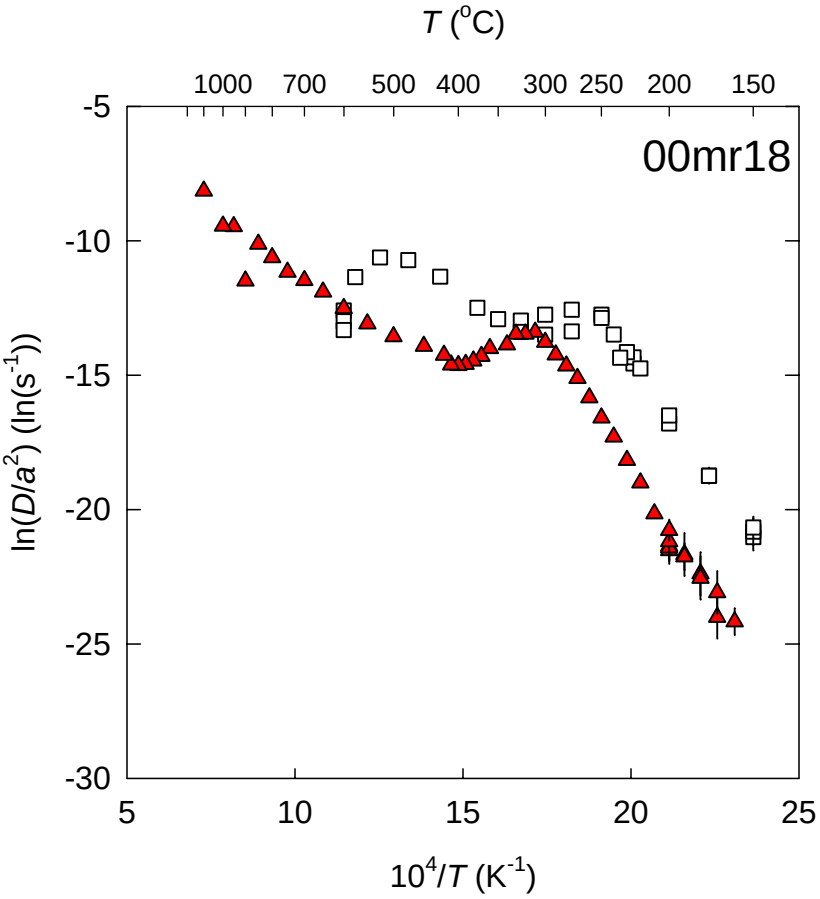

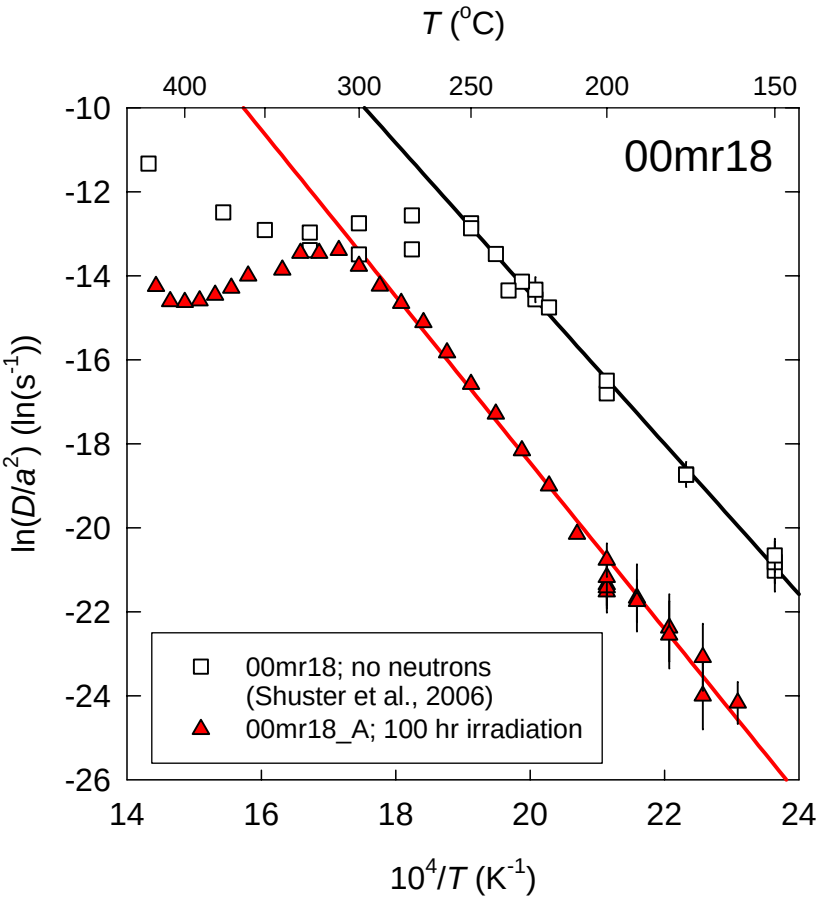

Shuster and Farley (2008)
Figure EA2a: 1 Hr (low temperatures)

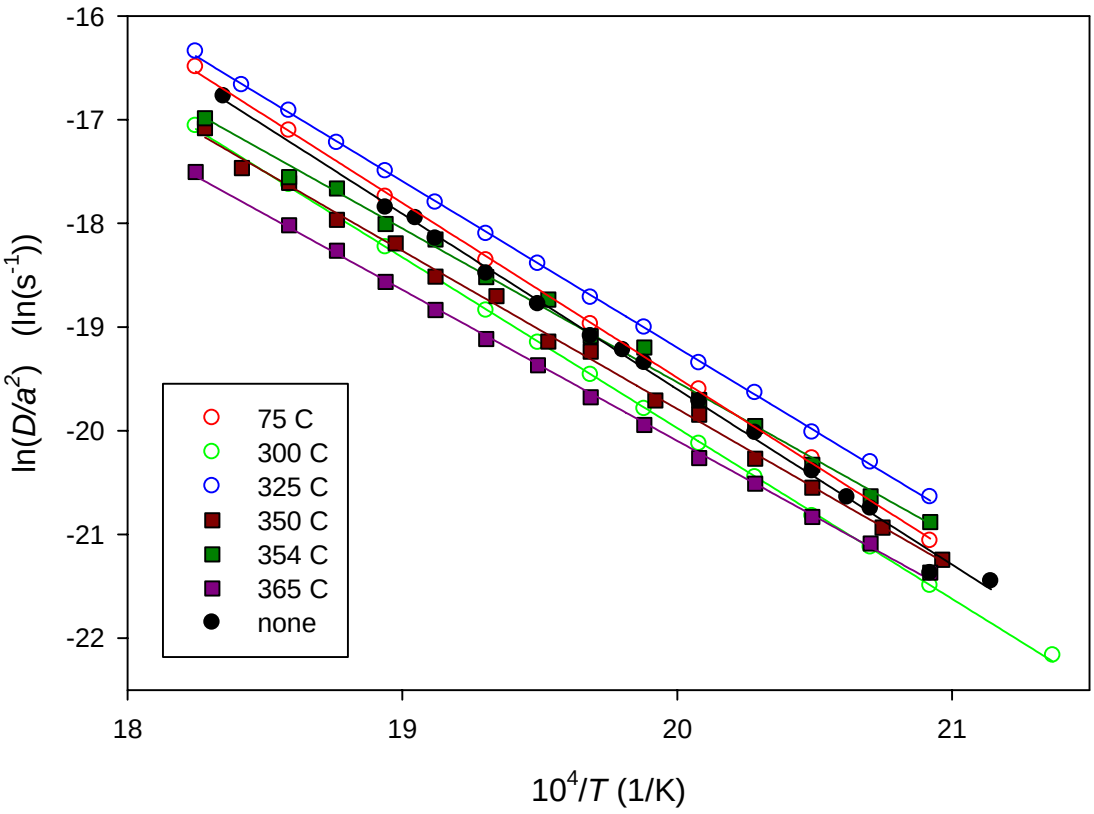

Shuster and Farley (2008)
Figure EA2b: 1 Hr (high temperatures)

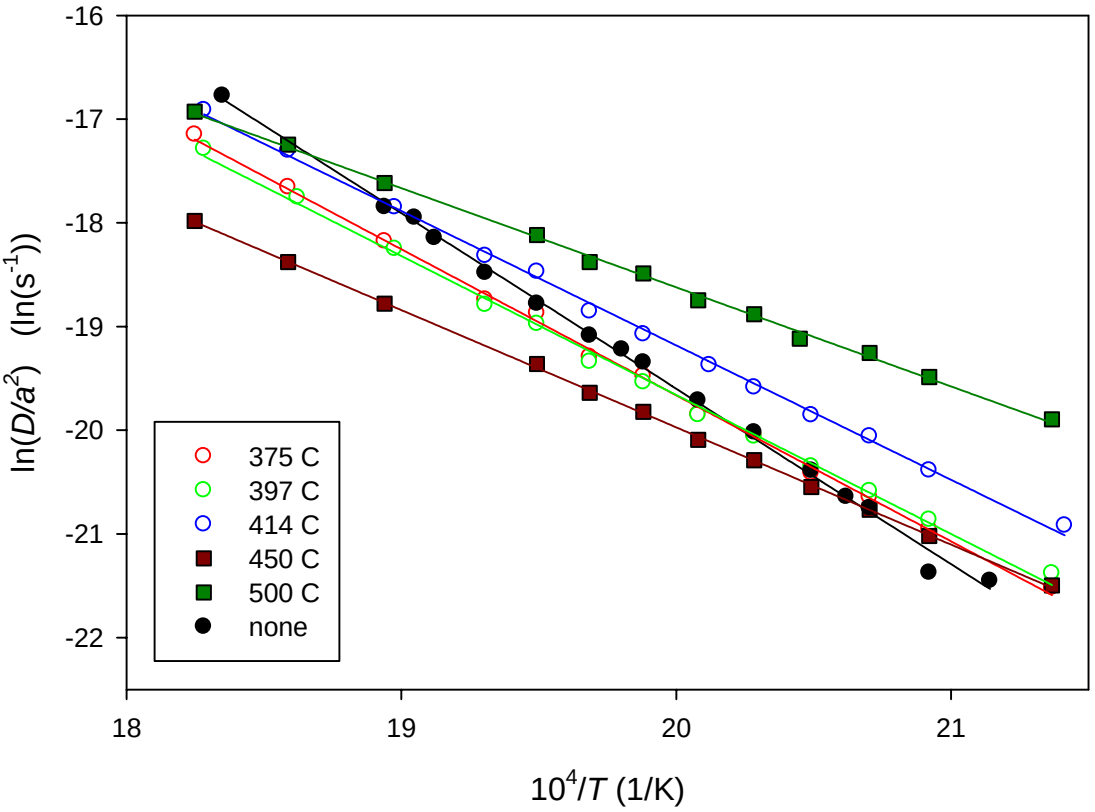

Shuster and Farley (2008)
Figure EA2c: 10 Hr

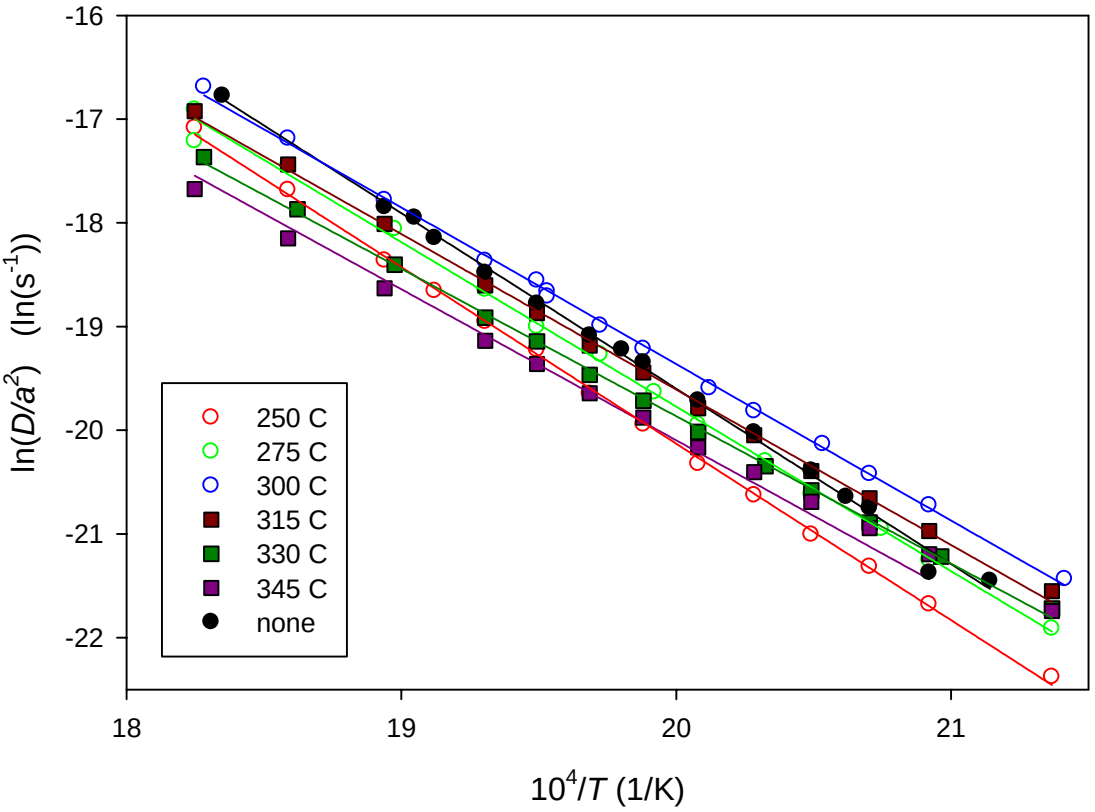

Shuster and Farley (2008)
Figure EA2d: 100 and 350 Hrs

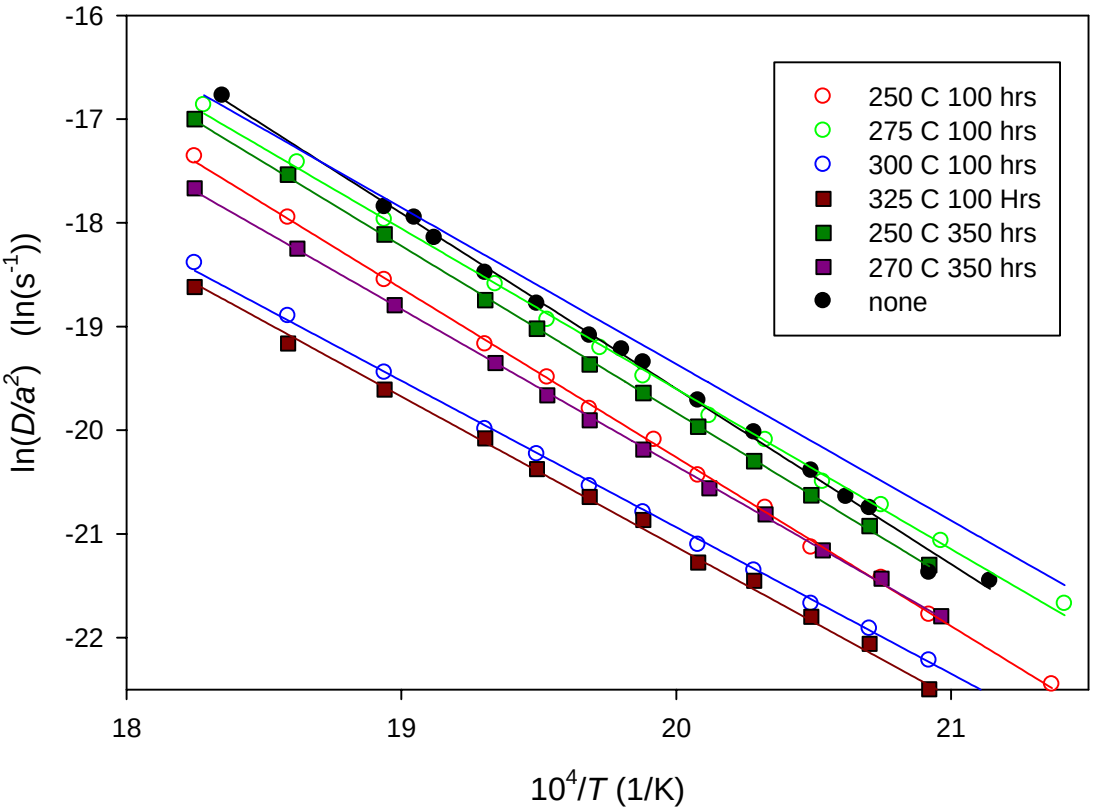

Shuster and Farley (2008)
Figure EA2e: 1 Hr, Chips

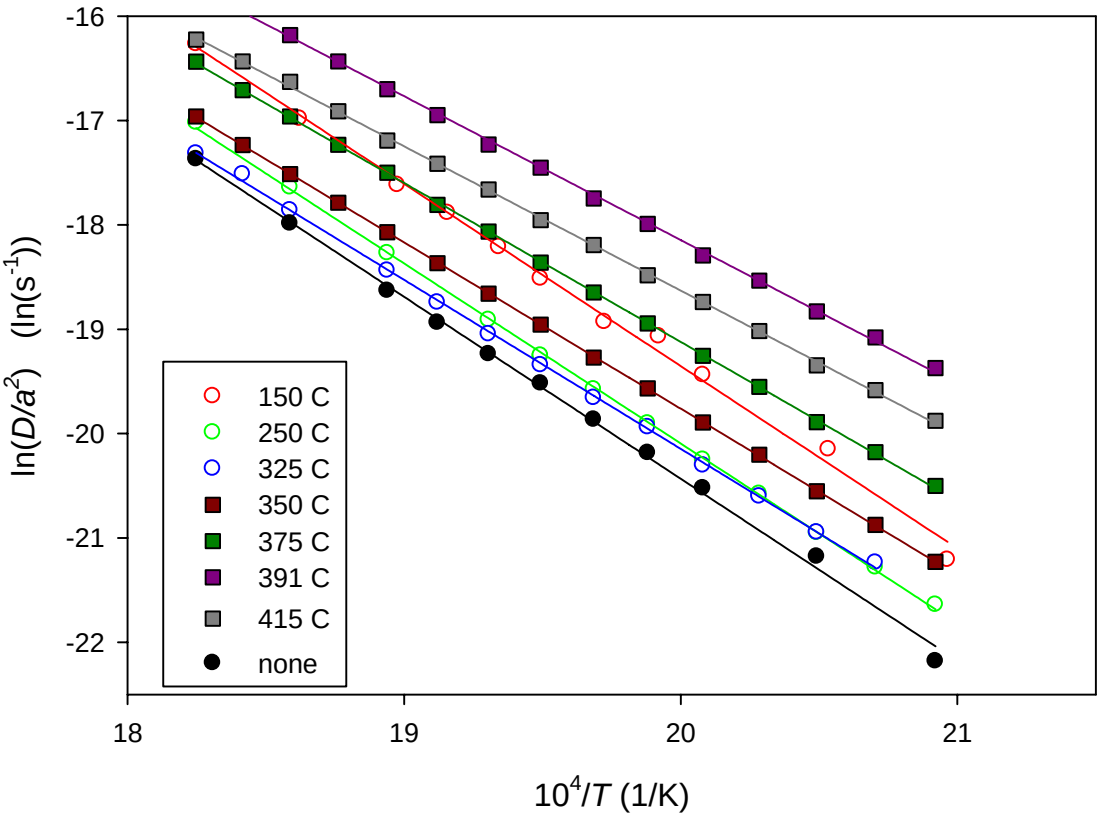

Shuster and Farley (2008)
Figure EA3

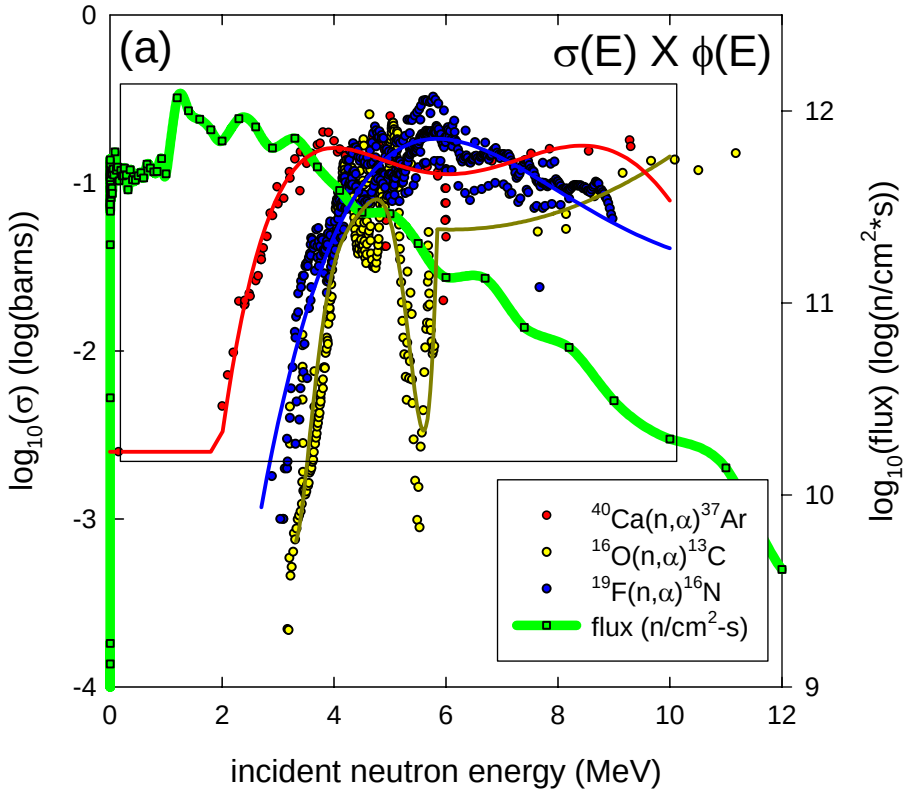

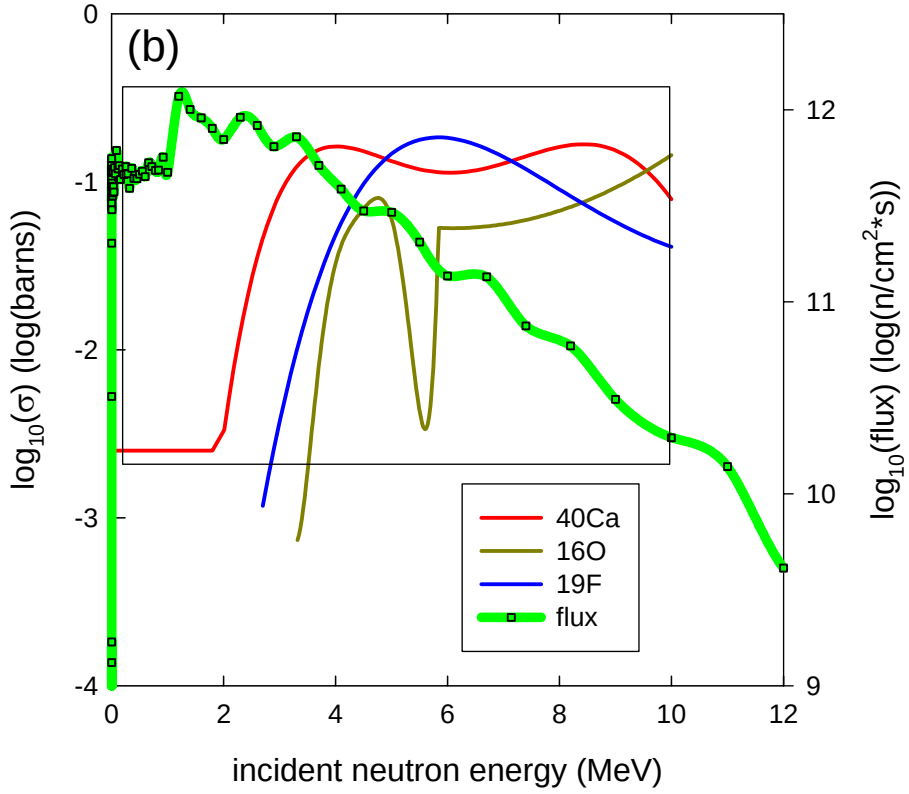

Shuster and Farley (2008)
Figure EA4

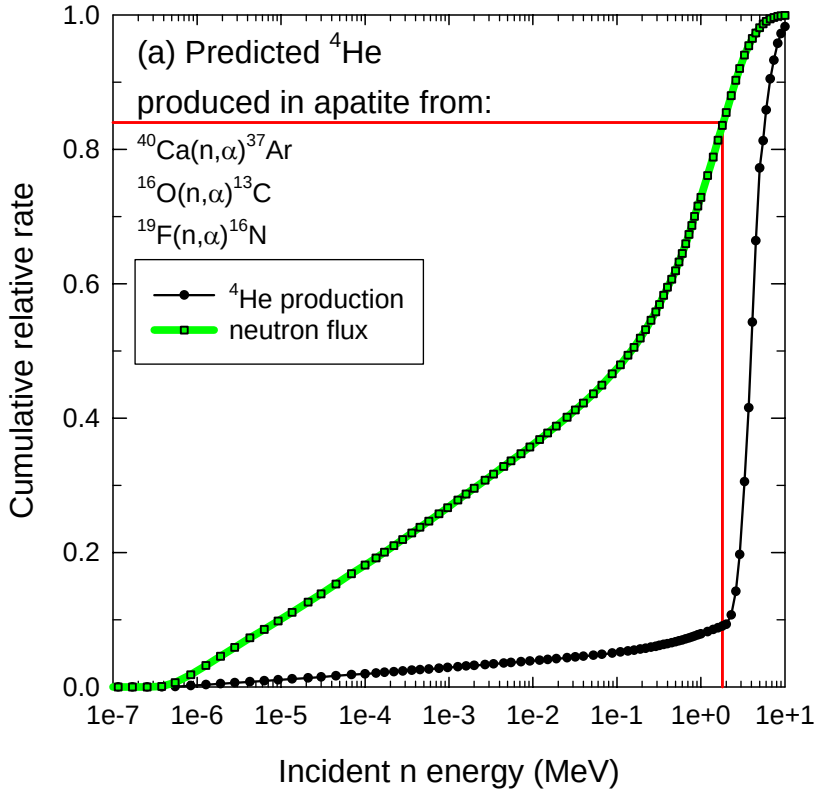

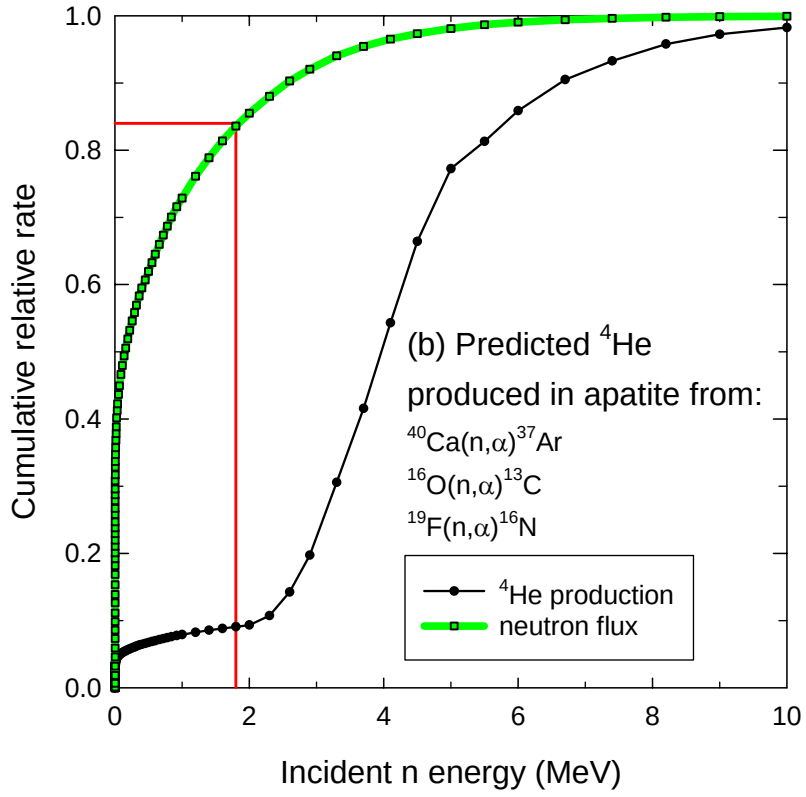

Shuster and Farley (2008)
Figure EA5